

Embedded Model Bias Quantification with Measurement Noise for Bayesian Model Calibration

Daniel Andrés Arcones^{a b *}, Martin Weiser^c, Phaedon-Stelios Koutsourelakis^b, Jörg F. Unger^a

^aBundesanstalt für Materialforschung und -prüfung, Berlin, Germany

^bTechnical University of Munich, Garching bei München, Germany

^cZuse Institute Berlin, Berlin, Germany

*Corresponding author: Daniel Andrés Arcones; daniel.andres-arcones@bam.de

15 October 2024

Abstract

The use of computer simulations to model physical systems has gained significant traction in recent years. A key factor in ensuring the accuracy of these models is the proper calibration of model parameters based on real-world observations or experimental data. Inevitably, uncertainties arise, and Bayesian methods provide a robust framework for quantifying and propagating these uncertainties to model predictions. However, predictions can become inaccurate if model errors are neglected. A promising approach to address this issue involves embedding a bias term in the inference parameters, allowing the quantified bias to influence non-observed Quantities of Interest (QoIs). This paper introduces a more interpretable framework for bias embedding compared to existing methods. Current likelihood formulations that incorporate embedded bias often fail when measurement noise is present. To overcome these limitations, we adapt the existing likelihood models to properly account for noise and propose two new formulations designed to address the shortcomings of the previous approaches. Moreover, we evaluate the performance of this bias-embedding approach in the presence of discrepancies between measurements and model predictions, including noise and outliers. Particular attention is given to how the uncertainty associated with the bias term propagates to the QoIs, enabling a more comprehensive statistical analysis of prediction reliability. Finally, the proposed embedded bias model is applied to estimate the uncertainty in the predicted heat flux from a transient thermal simulation, using temperature observations to illustrate its effectiveness.

Keywords: Model bias; Bayesian inference; noise; model updating; Quantity of Interest

Funding Statement This research was supported by the German Research Foundation (DFG) in the special focus program SPP 2388/1 “Hundert plus – Verlängerung der Lebensdauer komplexer Baustrukturen durch intelligente Digitalisierung” (Hundred Plus - Extending the service life of complex building structures through intelligent digitalisation) in the subproject C07: Data driven model adaptation for identification of digital twins of bridges.

1 Introduction

In the last decades, advances in sensor technology have made available large quantities of affordable data that reflects the current state of physical systems and processes. In parallel, simulation models have become ubiquitous in science and engineering for generating predictions on the behaviour of a given system based on physical laws. With the ongoing transition to an Industry 4.0 paradigm and the proliferation of Digital Twins, the challenge of calibrating simulation models based on data from physical sensors is becoming increasingly relevant (Vaidya et al. (2018)). In the specific case of Digital Twins of physical systems that use simulations to predict the behaviour of their real counterpart and make decisions on their behalf, the accuracy and reliability of such predictions are essential (Andrés Arcones et al. (2023)). Their uncertainty must be adequately quantified to achieve such trustworthy predictions.

In most cases, the calibration of the computational models is achieved by estimating a set of parameters that control its behaviour based on available observations from the modeled system. Although more uncertainty sources can be identified (Walker et al. (2003)), this process introduces two main ones: the error attributed to noise or uncontrolled variations in the data and the discrepancy created by the assumptions used to generate the computational model. They can be related to aleatoric and epistemic uncertainty sources, respectively. While noise

errors can be satisfactorily estimated from the observations, the so-called *model discrepancy* or *model inadequacy* presents further challenges. All models are based on assumptions and simplifications that are unavoidable when tackling an infinitely complex reality. Systematic reviews on different approaches for dealing with this model discrepancy exist (Bojke et al. (2009); Campbell (2006); Gupta et al. (2012); Pernot and Cailliez (2017); Sung and Tuo (2024)), but they all coincide in the need for further research to achieve reliable methods for quantifying the model uncertainty.

Bayesian approaches are usually implemented to infer the model parameters (Gelman et al. (2013); Robert (2007)), which allows to obtain a probability distribution for those parameters based on the observed data. This value will tend to converge to the optimal one for the computational model, which may not be able to represent the observations in the presence of model discrepancy (Kaipio and Somersalo (2006)). One classical solution to this problem is the framework proposed by Kennedy and O’Hagan in Kennedy and O’Hagan (2001), which extends the model output with a flexible term that corrects the predictions to better reflect the observations. Since its conception, several extensions have been proposed within the framework (Barbillon et al. (2024); Bayarri et al. (2009); Brynjarsdóttir and O’Hagan (2014); Leoni et al. (2024); Plumlee (2017)). However, one key disadvantage of such implementations is the impossibility of transferring the inferred estimation of the bias term to other derived Quantities of Interest (QoI) computed with the same calibrated model (Andrés Arcones et al. (2024)). In contrast to these *external* correction approaches that associate the uncertainty with the predictions from the model, *internal* corrections arise as an alternative by attributing the uncertainty to its components instead (Wu et al. (2024)). In this way, the inferred uncertainty can be pushed forward to any QoI that uses the same model parameters for its computation.

This family of approaches, also called Parameter Uncertainty Inflation (PUI) methods (Pernot (2017); Pernot and Cailliez (2017)) have been gaining traction in the last years. The most prominent approach is Sargsyan’s parameters embedding (Sargsyan et al. (2015); Sargsyan et al. (2019)), which adds a stochastic dimension to the variables to be inferred and fits it together with the other parameters. This methodology has been successfully implemented in the context of ignition reaction (Huan et al. (2017)). As alternatives to this methodology, Mortensen et al. (2005) proposes the statistical manipulation of the inferred parameter variance, and Wu et al. (2024) suggests inferring the internal model error structure through Kalman filters.

The aforementioned formulations have the advantage of offering a flexible implementation that can be adapted to the requirements of the problem. Despite being the most promising approach for dealing with model error through an internal correction, Sargsyan’s proposal requires further refinement for complex inference cases (Pernot (2017)). This paper aims to analyze the challenges that arise when using the embedded approach for the calibration of simulation models from sensor data, in particular the impact of misspecified noise models, the presence of observations that cannot be explained with modifications of the estimated parameter and the uncertainty propagation to other QoI. To alleviate the flaws of the two main likelihood formulations proposed in Sargsyan et al. (2015) for the embedded problem, the Independent Normal (IN) and Approximate Bayesian Computation (ABC) likelihoods, two additional formulations are proposed in this paper based on the statistical convergence of the residuals distribution: the Global Moment-matching (GMM) and Relative Global Moment-matching (RGMM) likelihoods. Additionally, further insight is provided for the choice in the control parameters of the likelihoods and their potential shortcomings. Finally, an analysis on the propagation of the uncertainties through QoI is developed.

The advantages and disadvantages of each formulation will be illustrated on a one-dimensional, linear example with different variations that reflect the possible errors in the observations. In the sequel, a more complex transient thermal model simulating the heat transfer through a reinforced concrete structure is investigated. The objective of the more complex case is to test the propagation of the inferred uncertainty to a non-related QoI. The structure of the rest of the paper is as follows. Section 2 presents the embedded approach, the likelihood functions and the proposed extensions. Section 3 includes the simple, linear model with its variations (Section 3.1) and the complex transient thermal one (Section 3.2). Conclusions and possible extensions are provided in Section 4.

2 Methodology

2.1 Model bias framework

Let f be a computable, deterministic function $f : \Theta \times \mathbb{R}^{n_x} \rightarrow \mathbb{R}^{n_z}$ for a n_x -dimensional input $x \in \mathbb{R}^{n_x}$, parametrized through a set of n_θ parameters $\theta \in \Theta \subseteq \mathbb{R}^{n_\theta}$, which have been restricted to real values for simplicity. This function f models the real response $z : \mathbb{R}^{n_x} \rightarrow \mathbb{R}^{n_z}$, defined as a real-valued map that generates the n_z -dimensional response of a real system. In that case, an additional error term $\varepsilon_{\text{model}} = z - f$ rooted on the inability of f to exactly reproduce z is introduced. This discrepancy term $\varepsilon_{\text{model}}$ will be referred to as *model bias*. If the same response is measured through sensor observations y , a noise $\varepsilon_{\text{noise}}$ will introduce an additional discrepancy with z . The relation between observations and computational model predictions can be expressed as

$$y = z(x) + \varepsilon_{\text{noise}} = f(\theta, x) + \varepsilon_{\text{model}} + \varepsilon_{\text{noise}}, \quad (1)$$

modeling the discrepancy terms additively. This formulation was introduced in the seminal paper of Kennedy and O’Hagan (2001), where they state the need for including the model error in the calibration of computational

models. Alternative formulations are possible, such as a multiplicative relation between discrepancy terms and model predictions.

The objective of the so-called *inverse problem* is to estimate the values for the parameters $\boldsymbol{\theta}$ such that f best approximates z as

$$\boldsymbol{\theta}^* = \arg \min_{\boldsymbol{\theta} \in \Theta} \|z - f(\boldsymbol{\theta}, \cdot)\|, \quad (2)$$

where $\|\cdot\|$ is a distance to be defined later. As z is not generally known, it is commonly substituted by the set of N sensor observations \mathbf{y} for known input parameters \mathbf{x} , where bold notation will be used to denote vector quantities. The inverse problem then transforms to

$$\boldsymbol{\theta}^* = \arg \min_{\boldsymbol{\theta} \in \Theta} \|\mathbf{y} - f(\boldsymbol{\theta}, \mathbf{x})\|. \quad (3)$$

Bayesian approaches are a popular choice to solve the inverse problem (Kaipio and Somersalo (2006)). They provide a posterior probability density $\pi(\boldsymbol{\theta}|\mathbf{y})$ on the parameters $\boldsymbol{\theta}$ given the observations \mathbf{y} and the computational model $f(\boldsymbol{\theta}, \mathbf{x})$. The application of Bayes' theorem yields

$$\pi(\boldsymbol{\theta}|\mathbf{y}) = \frac{\pi(\boldsymbol{\theta})\pi(\mathbf{y}|\boldsymbol{\theta})}{\pi(\mathbf{y})} \quad (4)$$

where $\pi(\boldsymbol{\theta}|\mathbf{y})$ is the *posterior* probability distribution, $\pi(\boldsymbol{\theta})$ is the *prior* probability distribution that encompasses the previous knowledge on the latent parameters, $\pi(\mathbf{y}|\boldsymbol{\theta})$ is the *likelihood* of the observations \mathbf{y} having been generated by $\boldsymbol{\theta}$ and $\pi(\mathbf{y})$ is the *marginal* probability distribution of the observations. We assume the prior distribution $\pi(\boldsymbol{\theta})$ to be given, such that the remaining key challenge is the choice and evaluation of the likelihood function $\mathcal{L}(\boldsymbol{\theta}) = \pi(\mathbf{y}|\boldsymbol{\theta})$ for the given set of observations \mathbf{y} . Bayesian inference approaches are based on the evaluation of the relationship from Equation 4 to obtain the posterior distribution of the latent parameters $\boldsymbol{\theta}$.

Once the posterior distributions of the latent parameters are obtained, they can be pushed forward to generate predictions $\mathbf{f}_P(\boldsymbol{\theta}, \mathbf{x}|\mathbf{y})$ using the same forward model f or they can be used in a different model $g(\boldsymbol{\theta}) : \Theta \rightarrow \mathbb{R}$, for example, that computes a QoI. In the first case $\mathbf{f}_P(\boldsymbol{\theta}, \mathbf{x}|\mathbf{y})$ can usually be compared with \mathbf{y} and indirectly $\mathbf{z}(\mathbf{x})$ through $\varepsilon_{\text{noise}}$.

The calculation of $\mathcal{L}(\boldsymbol{\theta})$ requires the evaluation of the computational model f under the assumption that it generates the real system's response z . However, that is not generally the case and the model error must be considered. Kennedy and O'Hagan (2001) propose to include the model bias $\varepsilon_{\text{model}}$ in the inference procedure formulated as a Gaussian Process added to the predicted response as in Equation 1. Despite its potential applications, this bias term lacks physical meaning and cannot be employed outside of the use case with which it is inferred. Notice that this bias term does not aim to identify the deficiencies in the model and correct them, but to introduce a term that envelops their effects such that the response is corrected.

More importantly, adding the bias term to the predicted outputs does not address one of the main challenges of using classical Bayesian inference approaches with imperfect models: the obtention of concentrated posterior distributions for the latent parameters whose associated pushed-forward model response could never have generated the observations, even for very large input datasets. Bernstein-von Mises theorem states that under a set of conditions of continuity, differentiability and non-singularity, the posterior distribution $\pi(\boldsymbol{\theta}|\mathbf{y})$ converges in total variation (TV) distance with the true generating process $\pi_{\boldsymbol{\theta}_0}$ to a multivariate normal distribution centered at the maximum likelihood estimator (MLE) $\hat{\boldsymbol{\theta}}$ and covariance matrix $N^{-1}\mathcal{I}(\boldsymbol{\theta}_0)^{-1}$. Here, N is the number of observations in \mathbf{y} and $\mathcal{I}(\boldsymbol{\theta}_0)$ is Fisher's information matrix at the true values $\boldsymbol{\theta}_0$ of the latent parameters (van der Vaart (2000)). Formally, this can be formulated as

$$\left\| \pi(\boldsymbol{\theta}|\mathbf{y}) - \mathcal{N}(\hat{\boldsymbol{\theta}}, N^{-1}\mathcal{I}(\boldsymbol{\theta}_0)^{-1}) \right\|_{TV} \xrightarrow{\pi_{\boldsymbol{\theta}_0}} 0. \quad (5)$$

This result is crucial for constructing confidence intervals for the parameters and predictive responses, linking Bayesian and frequentist statistics. For large values of N , the posterior distribution becomes concentrated around the MLE $\hat{\boldsymbol{\theta}}$. However, Kleijn and van der Vaart (2012) demonstrated that the confidence intervals derived from Bernstein-von Mises theorem application only reflect the real credibility of the predictions in the case of perfect models that can reproduce the observations exactly.

In the case of imperfect models, where discrepancies exist between the model and the data, the posterior distribution still converges to a multivariate normal distribution that concentrates around the MLE $\hat{\boldsymbol{\theta}}$ for large N . However, $\hat{\boldsymbol{\theta}}$ may not generate the observations due to the model discrepancy even for large N , and therefore the associated confidence intervals for the predictive response cannot be interpreted as credible intervals with respect to the true system, as demonstrated by Kleijn and van der Vaart (2012). This implies that the predicted distributions do not adequately capture the variability of the true system, making them unsuitable for quantifying system uncertainty.

When the bias term is implemented as a correction to the model response, the combined model $\mathbf{f}_P + \varepsilon_{\text{model}}$ (including the bias term) can reproduce exactly the observations \mathbf{y} . As a result, the Bernstein-von Mises theorem holds within the domain of the parameters updated during this process. However, the model \mathbf{f}_P alone cannot reliably quantify uncertainty without correction $\varepsilon_{\text{model}}$, which is limited to the observations' domain. Similar to the scenario where no bias term is used, the model produces overly concentrated posterior distributions for both

the parameters and the response, which may fail to represent the observations accurately. As the computation of QoIs through $g(\boldsymbol{\theta})$ usually depends only on the parameters and not on the corrected model response $\mathbf{f}_P + \varepsilon_{\text{model}}$, the uncertainty in the QoI will not be representative of the credibility of the model.

A promising solution to these challenges is the use of an embedded formulation where the bias is added to the model through the latent parameters. The objective is to augment those parameters with an additional stochastic variable that introduces aleatoric variations in the pre-existing model parameters. It is the introduction of this variability that prevents the latent parameters from presenting a concentrated posterior for large N . Following the same philosophy as Kennedy and O’Hagan’s (KOH) framework, no corrections are introduced in the structure of the physical model which allows the approach to be used non-intrusively with parametrized black-box models. This embedding is presented through Sections 2.2 to 2.4, the likelihood definition and evaluation in Sections 2.5 and 2.6, and the calculation of predicted variables through \mathbf{f}_P and QoIs through g are presented in Section 2.7.

2.2 Embedding of Model Bias

In many computational models, the latent parameters, denoted by $\boldsymbol{\theta}$, are treated as deterministic. However, in practice, these parameters often have uncertainties that can be better captured by replacing them with random variables, transforming the model into a stochastic framework. Therefore, we replace the deterministic latent parameters $\boldsymbol{\theta}$ by a random vector $\tilde{\boldsymbol{\theta}}$, and the task becomes identifying the distribution of $\tilde{\boldsymbol{\theta}}$ under some prior assumptions. This turns the originally deterministic model into a stochastic one, as it now depends on the random variable $\tilde{\boldsymbol{\theta}}$.

There are different ways to model the random vector $\tilde{\boldsymbol{\theta}}$. One well-known approach, due to Sargsyan et al. (2015) and Sargsyan et al. (2019), uses Polynomial Chaos Expansions (PCE) to represent the stochastic latent parameters. Specifically, the parameter vector $\tilde{\boldsymbol{\theta}}$ is expressed as a series expansion as

$$\tilde{\boldsymbol{\theta}} \sim \sum_j \alpha_j \Psi_j(\boldsymbol{\xi}), \quad (6)$$

where $\alpha_j \in \mathbb{R}^{n_\theta}$ are the expansion’s coefficients (included in the latent parameter space Θ), $\Psi_j : \mathbb{R}^{n_\xi} \rightarrow \mathbb{R}$ are orthogonal polynomials, and $\boldsymbol{\xi}$ is a set of stochastic variables (also called the stochastic germ) with $\boldsymbol{\xi} \in \mathbb{R}_{\xi}^{n_\xi}$ where n_ξ is the number of input random variables considered. This PCE-based approach allows for a flexible representation of the distribution of $\tilde{\boldsymbol{\theta}}$.

In this paper, we propose a more interpretable alternative. Instead of representing $\tilde{\boldsymbol{\theta}}$ as a polynomial expansion, we adopt an explicit representation where the stochasticity is introduced through an additive bias term. This approach is in line with the proposal of Oliver et al. (2015) for model error characterization and the work of Strong and Oakley (2014) on internal model discrepancies decomposition. Specifically, we model the random vector $\tilde{\boldsymbol{\theta}}$ as

$$\tilde{\boldsymbol{\theta}} = \boldsymbol{\theta}^m + \delta(\boldsymbol{\theta}^b), \quad (7)$$

where $\boldsymbol{\theta}^m$ represents the deterministic part, and $\delta(\boldsymbol{\theta}^b)$ is a parameterized zero-mean random vector that captures the stochastic deviation from $\boldsymbol{\theta}^m$. The parameters $\boldsymbol{\theta}^b$ control the magnitude of the stochasticity, and the explicit form of $\delta(\boldsymbol{\theta}^b)$ is chosen based on prior assumptions about the bias structure.

For simplicity, and because the exact shape of the distribution is often unknown, we assume that the bias $\delta(\boldsymbol{\theta}^b)$ follows a normal distribution. Specifically, we assume

$$\delta(\boldsymbol{\theta}^b) \sim \mathcal{N}(0, \text{diag}(\boldsymbol{\theta}^b)), \quad (8)$$

where $\boldsymbol{\theta}^b \in \mathbb{R}^{n_\theta}$ controls the variance of each parameter in $\tilde{\boldsymbol{\theta}}$. This formulation offers a clear interpretation of the bias associated with each parameter, making it easier to identify the sources of uncertainty and to calibrate the model accordingly.

Unlike the PCE approach, which implicitly incorporates bias through a series expansion and introduces many latent parameters for the PCE coefficients, our explicit bias representation offers a more direct and interpretable description of uncertainty. This is particularly valuable for model calibration, where identifying the sources of bias is crucial. Additionally, since the calculation of QoIs may only require some of the calibrated parameters, defining the embedded bias $\boldsymbol{\theta}^b$ independently for each parameter ensures that only the uncertainty associated with the relevant parameter is transferred. Separating the bias representation from the inference process also enables a more transparent treatment of uncertainty, reducing the identifiability issues that can arise when simultaneously fitting both the bias and model parameters.

For the remainder of this paper, we will use the formulation in Equation 7, assuming that $\delta(\boldsymbol{\theta}^b) \sim \mathcal{N}(0, \text{diag}(\boldsymbol{\theta}^b))$. Non-additive biases or biases with other probability distributions are possible, but they do not affect the generality of the method presented here. Variance structures with correlation can analogously be considered for δ . To generate a stochastic response from the computational model, the probability distribution of $\tilde{\boldsymbol{\theta}}$ must be pushed through the model. This presents computational challenges, as the forward model must be evaluated for each sample of $\tilde{\boldsymbol{\theta}}$. To address this, we implement a PCE approximation of the model’s response while keeping our identifiable embedding, which is detailed in Section 2.3.

Finally, because the model outputs are now stochastic, traditional inference methods that rely on deterministic outputs are no longer applicable. In Section 2.5, we introduce likelihood formulations in the spirit of Approximate

Bayesian Computation (ABC) methods that utilize summary statistics to infer the latent parameters of the model, providing a robust solution for stochastic models.

2.3 Forward model evaluation and Polynomial Chaos Expansion (PCE)

The evaluation of the stochastic response of the forward model requires the propagation of the uncertainty introduced by the embedding. A closed-form representation of the response is generally not possible, therefore sampling-based methods are required. A very popular approach for uncertainty propagation in recent years has been the use of generalized Polynomial Chaos Expansions (PCE) (Xiu and Karniadakis (2002)) to approximate the stochastic response once the uncertainty has been propagated. This approach consists of approximating the response f by a linear combination of a basis of orthonormal polynomials $\{\Psi_j\}_{j=0}^D$ truncated at degree d .

Let it be $\Psi_j : \mathbb{R}^{n_\xi} \rightarrow \mathbb{R}$, where $\xi \in \mathbb{R}^{n_\xi}$ and $n_\xi = n_b$, the number of input random variables. The number of polynomials D is computed as $D = \binom{d+n_b}{d}$, where n_b is the number of input random variables to be considered. Then, for each output $f_i(\theta) = f(\theta, x_i)$, which refers to the the model response evaluated at the i -th point x_i of the domain x (i.e., f_i is f evaluated at x_i with fixed θ), its approximation via PCE $\tilde{f}_i(\theta)$ is

$$f_i(\theta) \approx \tilde{f}_i(\theta) = \sum_{j=0}^D \alpha_{ij} \Psi_j(\xi) \quad (9)$$

To express this more concisely, the approximation can be written in vector form as

$$\mathbf{f}(\theta) \approx \tilde{\mathbf{f}}(\theta) = \sum_{j=0}^D \boldsymbol{\alpha}_j \Psi_j(\xi), \quad (10)$$

where α_{ij} are the PCE coefficients associated with each polynomial Ψ_j that fit the approximation to f_i (Sudret (2021)). The choice of the base of orthonormal polynomials Ψ depends on the distribution of the input random variables to be propagated. Askey's scheme (Xiu and Karniadakis (2002)) assigns popular distributions with their corresponding polynomial basis that ensures orthonormality and numerical stability. Additionally, PCE assumes independent input random variables, which can be enforced through the use of isoprobabilistic transformations such as Nataf or Rosenblatt transforms (Jakeman et al. (2019)).

Computing the α_{ij} coefficients requires solving the problem of minimizing the distance \mathcal{E} between $\mathbf{f}(\theta)$ and $\tilde{\mathbf{f}}(\theta)$ as in

$$\mathcal{E} = \left\| \mathbf{f}(\theta, x) - \tilde{\mathbf{f}}(\theta, x) \right\|_2 = \sqrt{\mathbb{E} \left[\mathbf{f}(\theta, x) - \tilde{\mathbf{f}}(\theta, x) \right]^2}. \quad (11)$$

Here, the α coefficients depend on x (the spatial domain), and the norm $\|\cdot\|_2$ is defined as the L_2 norm, with the inner product as:

$$\langle f, g \rangle = \int f(\xi)g(\xi)\pi_\xi(\xi) d\xi, \quad (12)$$

where $\pi_\xi(\xi)$ is the probability density function associated with ξ . The PCE coefficients that minimize \mathcal{E} are given by

$$\alpha_{ij} = \frac{1}{\langle \Psi_j, \Psi_j \rangle} \int_\xi f_i(\theta) \Psi_j(\xi) \pi_\xi(\xi) d\xi, \quad (13)$$

where $\pi_\xi(\xi)$ is the probability density associated with the random variable ξ . The term "stochastic germ" here refers to the random input variable, but "outcome" or "sample" could also be used. This integral can be computed using a Gauss quadrature scheme with weights w_1, w_2, \dots, w_P and nodes $\xi_1, \xi_2, \dots, \xi_P$, where $P = p^{n_b}$, the number of quadrature points. The expansion coefficients are then computed as

$$\alpha_{ij} = \frac{1}{\langle \Psi_j, \Psi_j \rangle} \sum_{k=1}^P w_k f_i(\theta(\xi_k)) \Psi_j(\xi_k) \pi_\xi(\xi_k), \quad (14)$$

where the factor $\pi_\xi(\xi_k)$ is included in the quadrature weights w_k .

The full process to evaluate a sample through the forward model is summarized in Algorithm 1. The Python package `chaospy` (Feinberg and Langtangen (2015)) has been used for the PCE implementation in this paper. The result of such evaluation is the PCE of the forward model's response, which is stochastic and requires post-processing. The polynomial formulation provides direct access to the statistical moments of the response. Let μ^h be the vector of means of the response $\tilde{\mathbf{f}}(\theta, x)$. Then, each of its entries can be obtained as

$$\mu_i^h = \mathbb{E} \left[\tilde{f}_i(\theta) \right] = \alpha_{i0}, \quad (15)$$

which holds under the assumption that $\Psi_0 = 1$. Analogously, the vector of variances σ^h is computed as

$$\left(\sigma_i^h \right)^2 = \text{Var} \left[\tilde{f}_i(\theta) \right] = \sum_{j=1}^D \alpha_{ij}^2, \quad (16)$$

because the variance is the sum of squares of the non-constant coefficients.

Algorithm 1 Forward model evaluation with Polynomial Chaos Expansion (PCE) and pseudo-spectral projection

Given a sample θ :

Step 1. Build a joint distribution \mathcal{J} of the stochastic latent parameters θ^b .

Step 2. If \mathcal{J} is not composed of independent variables, perform an isoprobabilistic transformation to make them independent, e.g., Nataf or Rosenblatt transform.

Step 3. Compute the weights w_1, w_2, \dots, w_D and nodes $\xi_1, \xi_2, \dots, \xi_D$ for the Gauss quadrature scheme of degree p given \mathcal{J} .

Step 4. Generate the orthonormal polynomial basis Ψ of degree d using Askey’s scheme.

Step 5. Evaluate the forward model at the nodes ξ for the sampled θ .

Step 6. For each entry in \mathbf{f} , compute the PCE coefficients α_j using Gauss integration with weights w , nodes ξ , and the corresponding model evaluations.

2.4 Embedded bias as a hierarchical Bayesian problem

The inverse problem with an embedded model bias can be interpreted within a hierarchical Bayesian framework. First, a set of *hyperpriors* is prescribed for θ^m and θ^b , from which they are sampled. Then, a prior distribution for θ is defined through Equation 7. Finally, the forward model is evaluated based on θ . This structure follows the sequential definition of latent variables that typically appears in hierarchical Bayesian models (Robert (2007)). This formulation can also be extended to use Approximate Bayesian Computation (ABC) (Turner and Van Zandt (2013)), which has been applied to inferring the modeling bias in industrial electric motor simulations (John (2021); John et al. (2021)). However, the classical hierarchical Bayesian framework fundamentally differs from the embedded approach in several key ways, both in implementation and computational efficiency.

This can be observed by comparing the posterior distribution for each approach. In the original embedded approach, the posterior distribution is expressed as:

$$\pi(\theta^m, \theta^b | \mathbf{y}) \propto \pi(\mathbf{y} | \theta^m, \theta^b) \pi(\theta^m, \theta^b). \quad (17)$$

Here, the stochastic vector of embedded variables $\tilde{\theta} = \theta^m + \delta(\tilde{\theta}^b)$ is not sampled nor treated as latent variables in the standard sense. Instead, the forward model $\mathbf{f}(\tilde{\theta}^m, \tilde{\theta}^b, \mathbf{x})$ produces a stochastic response directly, characterized by a distribution. This is achieved by pushing the uncertainty through the forward model using a PCE, which efficiently represents the random nature of $\delta(\tilde{\theta}^b)$ without requiring direct sampling of $\tilde{\theta}$.

In contrast, the posterior distribution in the hierarchical Bayes framework is expressed as

$$\pi(\theta^m, \theta^b | \mathbf{y}) \propto \pi(\mathbf{y} | \tilde{\theta}) \pi(\tilde{\theta} | \theta^m, \theta^b) \pi(\theta^m, \theta^b). \quad (18)$$

In practice, this approach necessitates access to and sampling from the conditional distribution $\pi(\tilde{\theta} | \theta^m, \theta^b)$, often requiring iterative methods like Gibbs sampling (Robert (2007); Robert and Casella (2004)), which increases computational cost. Often a sample $\tilde{\theta}_s$ is drawn from the conditional distribution $\pi(\tilde{\theta} | \theta^m, \theta^b)$. The forward model \mathbf{f} is evaluated for $\tilde{\theta}_s$ as $\mathbf{f}(\tilde{\theta}_s, \mathbf{x})$, and the response is deterministic.

The differences can be visualized in the Bayesian graphs in Figure 1, where the bias in a single parameter $\tilde{\theta}$ is modeled such that $\tilde{\theta} = \theta^m + \delta(\tilde{\theta}^b)$, where $\delta \sim \mathcal{N}(0, \sigma_\delta)$. Equivalently, $\tilde{\theta} \sim \mathcal{N}(\theta^m, \sigma_\delta)$ for this simple case. This highlights that both the embedded and hierarchical formulations can be implemented similarly, but the main difference lies in how the forward model response is treated. The embedded approach handles it stochastically, leveraging the PCE, while the hierarchical Bayes approach leads to a deterministic forward model after sampling $\tilde{\theta}$.

In simple cases such as the one presented in Figure 1, the advantages of using an embedding approach over a hierarchical one may not be obvious. However, as the number of parameters and levels of dependency increases, the hierarchical approach necessitates further nested iteration loops for sampling conditional distributions, which often results in slower convergence rates. In contrast, the embedding approach reduces this issue by sampling all variables only once, albeit at the cost of introducing more complex polynomial chaos expansion (PCE) structures. Nonetheless, the curse of dimensionality associated with PCE can be mitigated using sparse integration schemes Constantine et al. (2012).

A significant consequence of the stochastic nature of the response in the embedded approach is that classical likelihood models commonly employed in hierarchical Bayesian models are not directly applicable. Instead, PCE facilitates rapid computation of moments, which can be utilized for moment-matching likelihood computations inspired by approximate Bayesian computation (ABC) methods. By explicitly fitting the statistical moments of the predictions, this approach offers additional insights and enhances control over the update procedure compared to the hierarchical approach.

Hierarchical methods may be preferable in scenarios where efficiently sampling the conditional distributions of latent parameters is feasible. This is particularly true for cases with a limited number of parameters or complex stochastic structures requiring higher-degree polynomials in the PCE for accurate approximation. In these situations, despite the expected slower convergence rates of hierarchical Bayesian methods using iterative

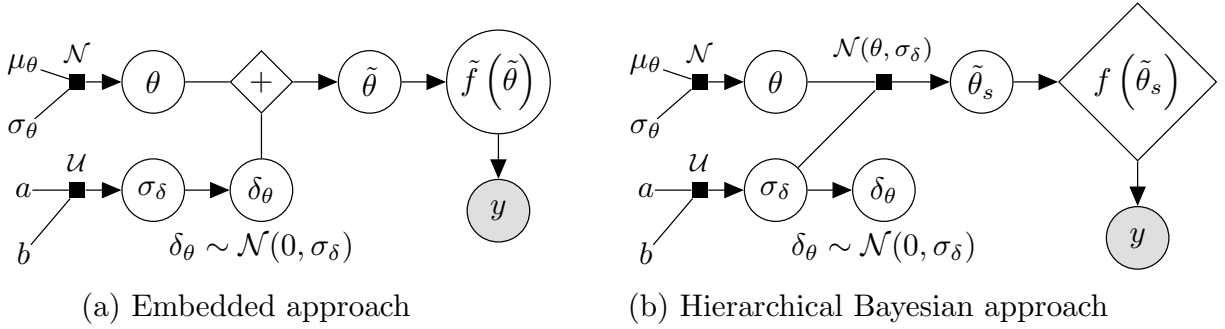


Figure 1: Bayesian graph for the inference of the parameters involved in the embedded formulation of the model bias. (a) Embedded approach. (b) Classical hierarchical Bayesian approach with Gibbs’ sampling. Following usual notation (Dietz (2010); Obermeyer et al. (2019)), circled values with white background represent latent variables, circled shaded values represent observations, rhomboids represent deterministic operations, and black squares represent drawing a sample from the indicated distribution. In this case, $\theta \sim \mathcal{N}(\mu_\theta, \sigma_\theta)$ and $\sigma_\delta \sim \mathcal{U}(a, b)$. Notice that the main different roots in $\tilde{\theta}$ being sampled in (b) but not in (a). This leads the response $\tilde{f}(\tilde{\theta})$ to be a stochastic variable in (a) obtained from pushing the distribution of $\tilde{\theta}$ through f by building the PCE; but in (b) a deterministic response $f(\tilde{\theta}_s)$ is obtained for the sampled $\tilde{\theta}_s$.

algorithms, they may still outperform the embedding approach due to the additional forward model evaluations required.

While both methodologies have practical applications, an exhaustive comparison between them is beyond the scope of this paper. For a more comprehensive discussion on hierarchical Bayesian approaches and their computational challenges, refer to Li et al. (2024); Robert (2007); Robert and Casella (2004); Turner and Van Zandt (2013).

2.5 Likelihood formulation

Due to the uncertainty propagation, the output of a given evaluation of the forward model $\tilde{f}(\theta)$ for a sampled θ is stochastic in nature and follows a probability distribution described by the PCE approximation. While a modified approach that utilizes the statistical moments of the distribution is feasible, directly evaluating a classical Gaussian likelihood function based on the residuals between the predictions, $\tilde{f}(\theta)$, and the observations, \mathbf{y} , is not possible because their domains are not directly comparable. Approximate Bayesian Computation (ABC) approaches provide a methodology to obtain the likelihood $\pi_{\text{ABC}}(\mathbf{y}|\theta)$ from the statistical moments of $\tilde{f}(\theta)$, which are readily available from the PCE.

Throughout this paper, an ensemble-based MCMC sampler using a stretch move (Goodman and Weare (2010)) from the package `emcee` (Foreman-Mackey et al. (2013)) is used, therefore the likelihood functions will be implemented in this context. A threshold on the *effective sample size* (*ESS*) for each of the latent parameter chains as described in Appendix A is set as stopping criteria for the MCMC algorithm.

2.5.1 ABC-Likelihood without noise

Classical ABC approaches usually include two assumptions: (1) measurements are free of noise, $\varepsilon_{\text{noise}} \stackrel{!}{=} 0$, and (2) the model response can fully represent the system, $\varepsilon_{\text{model}} \stackrel{!}{=} 0$. Therefore, the model response is expected to fully represent the system’s real behaviour as $\mathbf{z} = \mathbf{f}(\theta)$. Those approaches include the following steps (Sisson et al. (2018)):

1. Sample θ from $p(\theta)$.
2. Evaluate the forward model $\mathbf{z} = \mathbf{f}(\theta) \sim p(\mathbf{z}|\theta)$.
3. Accept or reject θ if $\rho(\mathbf{y}, \mathbf{f}(\theta)) < \epsilon$.

If the model is approximated, such as the forward model built in Section 2.3, its evaluation would correspond to $\tilde{\mathbf{z}} = \tilde{\mathbf{f}}(\theta) \sim p(\tilde{\mathbf{z}}|\theta)$, where the model bias is expected to be fully represented in the stochastic response of the computational model, preserving assumption (2). The distance $\rho(\mathbf{y}, \tilde{\mathbf{f}}(\theta)) : \mathbb{R}^{n_y} \times \mathbb{R}^{n_z} \rightarrow \mathbb{R}$, is defined between observations and predictions and the objective of the approach is to reduce it under a tolerance value ϵ . When this tolerance $\epsilon \rightarrow 0$, the predictions are expected to reproduce exactly the observations, and therefore the samples of θ would belong to the associated posterior distribution. As \mathbf{y} is deterministic and $\tilde{\mathbf{f}}(\theta)$ stochastic, the distance ρ is evaluated on its statistical moments t such that

- 3a. Accept or reject θ if $\rho(t(\mathbf{y}), t(\tilde{\mathbf{f}}(\theta))) < \epsilon$.

A possibility is to use the mean and standard deviation as summary statistics under the assumption of them being statistically *sufficient*. The predictions $\tilde{\mathbf{f}}(\boldsymbol{\theta})$ are approximated at each output dimension by $t(\tilde{\mathbf{f}}(\boldsymbol{\theta})) = [\boldsymbol{\mu}^h, \boldsymbol{\sigma}^h]$. The output observations \mathbf{y} are approximated by its statistical moments as $t(\mathbf{y}) = [\boldsymbol{\mu}, \boldsymbol{\sigma}]$, where $\boldsymbol{\mu} \approx \mathbf{y}$ and $\boldsymbol{\sigma} \approx \gamma|\boldsymbol{\mu}^h - \mathbf{y}|$ with γ an additional factor to be specified. The approximation $\boldsymbol{\sigma} \approx \gamma|\boldsymbol{\mu}^h - \mathbf{y}|$ is necessary due to only one observation being available. A reasonable assumption would be that on, average, the observations \mathbf{y} are located a given distance from the mean $\boldsymbol{\mu}^h$ controlled by their standard deviations $\boldsymbol{\sigma}$, leading to the previous approximation. The choice of summary statistics is not unique and introduces a potential discrepancy rooted in the approximation that is not present in the formulation (Fearnhead and Prangle (2012)).

The acceptance criterion defines the *indicator function* or *kernel* that governs the sampling procedure. Following the criteria from Step 3, the uniform kernel I indicates if a sample is accepted and can be defined as

$$I(\boldsymbol{\theta}, \mathbf{y}) = \begin{cases} 1 & \text{if } \rho(t(\mathbf{y}), t(\tilde{\mathbf{f}}(\boldsymbol{\theta}))) < \epsilon \\ 0 & \text{else} \end{cases}. \quad (19)$$

Applying Bayes' theorem with the chosen kernel, it is possible to express the approximate posterior distribution of the parameters as

$$\pi_{\text{ABC}}(\boldsymbol{\theta}|\mathbf{y}) \propto \pi(\boldsymbol{\theta}) \int_{\mathbb{R}^{n_z}} I(\boldsymbol{\theta}, \mathbf{y}) \pi(\mathbf{z}|\boldsymbol{\theta}) d\mathbf{z} \quad (20)$$

where $\pi(\boldsymbol{\theta})$ is the prior distribution for the latent parameters $\boldsymbol{\theta}$ and $\pi(\mathbf{z}|\boldsymbol{\theta})$ the probability of the model output for a given $\boldsymbol{\theta}$. For a deterministic model f , the probability $\pi(\mathbf{z}|\boldsymbol{\theta})$ follows a Dirac's delta distribution located at the value for $\mathbf{f}(\boldsymbol{\theta})$. Analogously, the summary statistics $t(\tilde{\mathbf{z}})$ of the approximated output $\tilde{\mathbf{z}} = \mathbf{f}(\boldsymbol{\theta})$ are deterministic as well, therefore $\pi(t(\tilde{\mathbf{z}})|\boldsymbol{\theta})$ follows the same Dirac's delta distribution when they are used as a lower-dimensional representation of the model output. Under this consideration, it can be observed that the kernel acts as the likelihood function that is commonly defined in the classical Bayesian approaches. In particular, the likelihood defined by the aforementioned uniform kernel assigns probability 1 to those samples that fulfil $\rho(t(\mathbf{y}), t(\tilde{\mathbf{z}})) < \epsilon$ and 0 elsewhere.

Following the same reasoning, it is possible to implement other likelihood functions that reciprocally induce different kernels that govern the acceptance criteria. Such is the case for the *moment-matching* likelihood used in Sargsyan et al. (2015) and Sargsyan et al. (2019), which adopts an exponential structure:

$$\mathcal{L}^{\text{ABC}}(\boldsymbol{\theta}) = (2\pi\epsilon^2)^{-\frac{1}{2}} \prod_{i=1}^{n_y} \exp\left(-\frac{(\mu_i^h - y_i)^2 + (\sigma_i^h - \gamma|\mu_i^h - y_i|)^2}{2\epsilon^2}\right) \quad (21)$$

hence

$$\pi_{\text{ABC}}(\boldsymbol{\theta}|\mathbf{y}) \propto \pi(\boldsymbol{\theta}) \mathcal{L}^{\text{ABC}}(\boldsymbol{\theta}). \quad (22)$$

This likelihood assigns higher probabilities to those samples that minimize the squared distance between the summary statistics $[\boldsymbol{\mu}^h, \boldsymbol{\sigma}^h]$ and the observations, defined as

$$\rho(t(\mathbf{y}), t(\tilde{\mathbf{f}}(\boldsymbol{\theta}))) = \begin{bmatrix} \boldsymbol{\mu}^h - \mathbf{y} \\ \boldsymbol{\sigma}^h - \gamma|\boldsymbol{\mu}^h - \mathbf{y}| \end{bmatrix}^T \begin{bmatrix} \boldsymbol{\mu}^h - \mathbf{y} \\ \boldsymbol{\sigma}^h - \gamma|\boldsymbol{\mu}^h - \mathbf{y}| \end{bmatrix}. \quad (23)$$

While this distance has demonstrated convergence, it is primarily influenced by the statistical moment with the largest variance (Prangle (2017)). Notably, the value of $\boldsymbol{\mu}^h$ is mainly affected by variations in the original latent parameters, whereas $\boldsymbol{\sigma}^h$ is contingent upon the latent parameters associated with the embedded bias. The moment-matching likelihood is justified by the assumption of normality in the differences between the predicted summary statistics and those of the observations. The goal is to achieve an exact match between the predicted and observed statistical moments, which occurs as ϵ approaches 0, assuming there is no model discrepancy—that is, when the model can perfectly replicate the real system. When the measurement noise ϵ_{noise} is either zero or can be completely absorbed by the model bias, the posterior predictive distribution generated using this likelihood converges to the true distribution, provided that the summary statistics are sufficient.

The choice of γ is also not trivial and depends on the assumptions imposed on the residuum's distribution. It can be argued that, supposing a normal independent probability distribution for the residuum, $\gamma = \sqrt{\frac{\pi}{2}}$ should be chosen over $\gamma = 1$ if the desired expected predictive distribution is supposed to have, on average, the magnitude of the residuum as the standard deviation. For a variable u that follows a zero-mean normal distribution $u \sim \mathcal{N}(0, \sigma)$, its absolute value $|u|$ follows a half-normal distribution (Gelman et al. (2013); Leone et al. (1961)), and therefore

$$\mathbb{E}[|u|] = \sigma \sqrt{\frac{2}{\pi}}. \quad (24)$$

Therefore, if $\boldsymbol{\sigma}^h$ on average should be equal to the residuum $\boldsymbol{\mu}^h - \mathbf{y}$ at every point and not to the expectation of $|\boldsymbol{\mu}^h - \mathbf{y}|$, a correction of $\gamma = \sqrt{\frac{\pi}{2}}$ is required. In such case, the residuum obtained from the observations is, on average, one standard deviation $\boldsymbol{\sigma}^h$ from the mean. Sargsyan et al. (2019) proposes taking $\gamma = 1$ as a general case instead, specifying then $\boldsymbol{\sigma} \approx |\boldsymbol{\mu}^h - \mathbf{y}|$, observing that alternative values of γ should be informed by knowledge on the system (Sargsyan et al. (2019)). However, for the likelihood of Equation 21 that would imply underestimating the predictive variance. Further discussion on the impact of modifying γ and ϵ for this likelihood can be found in Sargsyan et al. (2015). Equation 22 can be implemented in an MCMC framework to estimate the posterior distribution (Marjoram et al. (2003); Sisson and Fan (2010)).

2.5.2 ABC-Likelihood with noise

The likelihood formulated in Equation 21 does not explicitly include the measurement noise that appears in the observations. It supposes that the moments can be matched exactly up to a constant ϵ , which in reality is generally not true. In cases where measurement noise is present, it is not possible to reduce ϵ to zero, which invalidates the moment-matching condition and introduces an error in the posterior. Therefore, the explicit inclusion of noise is required to generate a reliable posterior based on real sensor observations.

Three main alternatives have been proposed by Schälte and Hasenauer (2020) to include noise in ABC approaches: (1) controlling the noise through ϵ , (2) simulating samples from the noisy model $f(\theta) + \varepsilon_{\text{noise}}$ and (3) including the noise model in the sample acceptance criteria, and therefore the likelihood function. Fitting the tolerance to the expected noise is not trivial, as the variation in the summary statistics does not necessarily coincide with the prescribed measurement noise, and it limits the application to uniform noise models (Daly et al. (2017)). Alternatively, simulating samples leads to low acceptance rates and largely increases the number of required model evaluations per sample. Finally, the modification of the acceptance criteria has been proven to correctly converge to the posterior of the summary statistics with noise (Wilkinson (2013)). Based on this property, a modification to include the noise in the moment-matching likelihood function is proposed here.

Following Wilkinson (2013), the acceptance step of the general ABC outline is modified to include the noise error:

- 3b. Accept θ with probability $\frac{\pi_\epsilon(t(\mathbf{y}) - t(\tilde{\mathbf{z}}))}{c}$.

where $\pi_\epsilon(t(\mathbf{y}) - t(\tilde{\mathbf{z}}))$ represents the probability error model for the summary statistics and c is a normalization constant. Applying the MCMC framework and using $\pi_\epsilon(t(\mathbf{y}) - t(\tilde{\mathbf{z}}))$ as likelihood, the posterior distribution of the latent parameters can be approximated as

$$\pi_{\text{ABC}}(\theta, \mathbf{z}|\mathbf{y}) \approx \pi_{\text{ABC}}(\theta, t(\mathbf{z})|t(\mathbf{y})) \propto \pi_\epsilon(t(\mathbf{y}) - t(\tilde{\mathbf{z}}))\pi(\theta). \quad (25)$$

The proof of convergence is presented in Appendix B under consideration that $t(\tilde{\mathbf{z}}) = t(\tilde{\mathbf{f}}(\theta))$ is deterministic. This holds true, as a given sample θ will produce the same statistical moments for the pushed-forward distribution as defined in the PCE approximation.

The chosen summary statistics are the same as for the original moment-matching likelihood: the mean and standard deviation of the model. The error $\varepsilon_{\text{noise}} = \mathbf{y} - \tilde{\mathbf{z}}$ follows a prescribed homogeneous Gaussian noise model $\mathcal{N}(0, \sigma_N \mathbf{I})$. Therefore, the noise associated with the means has variance σ_N^2 . On the other hand, the matching of predicted and estimated standard deviations is considered exactly up to the tolerance ϵ . The predicted standard deviation now not only considers the variation in the output σ^h but also includes the noise vector σ_N . Therefore, the second moment comparison with noise is $\sigma = \sigma^h + \sigma_N \approx \gamma|\mu^h - \mathbf{y}|$. With this new formulation, the variance in the residuals $\mathbf{u} = |\mu^h - \mathbf{y}|$ will be explained by the prescribed measurement error first if possible, and the predicted variance would intuitively only be increased to cover for the remaining variance. For the aforementioned homogenous Gaussian error, the noisy moment-matching likelihood function is

$$\mathcal{L}^{\text{ABC}}(\theta) = (2\pi\epsilon^2\sigma_N^2)^{-\frac{n_y}{2}} \prod_{i=1}^{n_y} \exp\left(-\frac{(\mu_i^h - y_i^h)^2}{2\sigma_N^2} - \frac{(\sigma_i^h + \sigma_N - \gamma|\mu_i^h - y_i^h|)^2}{2\epsilon^2}\right). \quad (26)$$

This modified likelihood presents several advantages in the case of measurements with noise. First and most prominently, the predicted and sampled means are no longer matched exactly, as their fitness is evaluated considering the known measurement noise structure. This avoids over-fitting to the samples and provides more informative posterior distributions that consider a larger part of the available information. Additionally, the variance from measurement noise is no longer absorbed by the stochastic part of the model prediction, which avoids overestimating the model bias.

Nevertheless, both moment-matching likelihoods are sensitive to badly represented models. As proven in C, if the prescribed noise is larger than the residuals, the inference procedure will converge to a posterior distribution that not necessarily represents the real system. This occurs when the sampling algorithm favours samples with a larger residual in order to exactly match the standard deviation of the prediction with the prescribed noise model. However, this situation can be avoided by a careful selection of the prescribed noise model, as is generally the case in practice. Alternatively, the noise parameter can be inferred as a latent parameter, which is possible only for the noisy moment-matching likelihood function.

2.5.3 Global Moment-matching Likelihood with noise

The *Global Moment-matching Likelihood* (GMM) aims to calculate the distance between the expected statistical moments of the whole simulation dataset and the predicted ones, instead of evaluating the fitness point-wise. Therefore, the summary statistics to be matched will be the first and second statistical moments of the whole distribution. We will work under the assumption that each individual sample, i.e. each observation-prediction pair and a given θ , generates a residual error that is drawn from a common normal distribution such that, at each single sample of coordinates x ,

$$\varepsilon(\theta) = y(x) - f(\theta, x), \quad \varepsilon(\theta) \sim \mathcal{N}(\mu_\varepsilon, \sigma_\varepsilon). \quad (27)$$

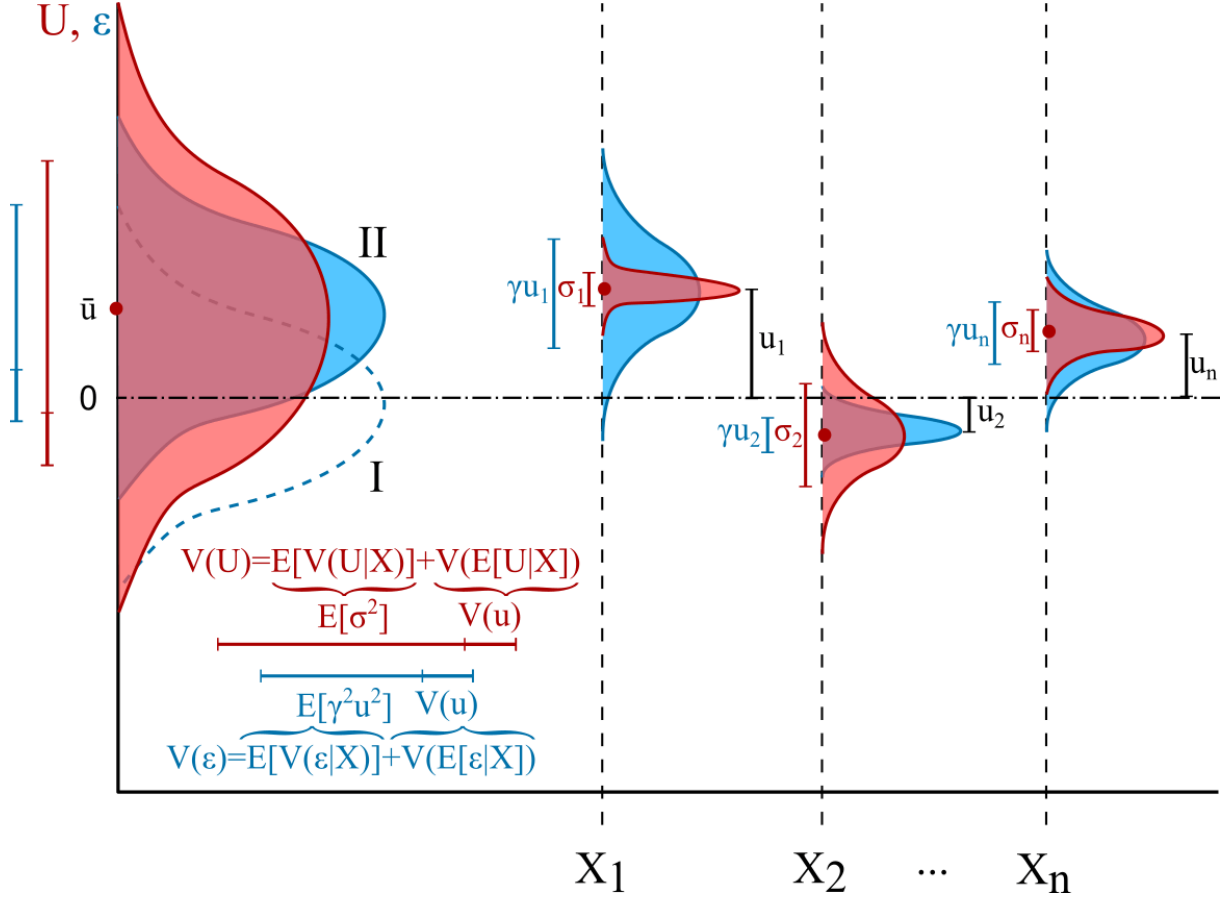


Figure 2: Summary of GMM and RGMM likelihood formulations. For each sampled X_i , a “sampled” predictive distribution (in red) of the residual u_i is obtained. Additionally, a “population” predictive distribution is defined with the belief of the expected distribution. Then, the whole sample set is built by adding the sampled predictive distributions, obtaining a distribution with mean \bar{u} and variance s_ε^2 . Analogously, the individual population distributions are added to get a population set distribution. The moments of the sampled set distribution are matched to obtain zero mean given the population set variance (I) and sample variance asymptotically equal to the one of the population set (II). The difference between GMM and RGMM is the use of absolute or relative residuals.

Using the same normal approximation for the whole population allows the inclusion of the noise directly in the residual distribution and avoids having to specify a tolerance ϵ . This assumption is generally not true, as each sample may present different residuals based on how well the predictions are fitted at that given x . For specific cases it could be a reasonably good approximation for the set of all samples. The values for μ_ε and σ_ε are prescribed for a given θ and can be interpreted as the target population parameters. In this paper, the target population is defined such that it minimizes the residual between observations and predictions ($\mu_\varepsilon = 0$), and that the standard deviation σ_ε of the samples represents the discrepancy generated by the model misspecification and noise. A summary representation of the basis of GMM likelihood is represented in Figure 2.

The variance σ_ε^2 for a given value of θ can be obtained by applying the total variance theorem conditioned by the samples as

$$\sigma_\varepsilon^2 = \text{Var}(\varepsilon(\theta)) = \underbrace{\mathbb{E}[\text{Var}(\varepsilon|x)]}_{\text{Within-sample variance}} + \underbrace{\text{Var}(\mathbb{E}[\varepsilon|x])}_{\text{Between-sample variance}}. \quad (28)$$

For a given sample of coordinates x , the expectation and variance of the residual error are

$$\mathbb{E}[\varepsilon|x] = y(x) - \mu^h(x) = u \quad (29)$$

$$\text{Var}(\varepsilon|x) = \sigma_{\text{model}}^2 + \sigma_N^2, \quad (30)$$

where u is the residuum for the given x and θ , σ_{model}^2 is the model’s variance and σ_N^2 the prescribed noise variance. The within- and between-sample variances are then

$$\mathbb{E}[\text{Var}(\varepsilon|x)] = \overline{\sigma_{\text{model}}^2 + \sigma_N^2} = \overline{\sigma_{\text{model}}^2} + \sigma_N^2 \quad (31)$$

$$\text{Var}(\mathbb{E}[\varepsilon|x]) = \text{Var}(u) \quad (32)$$

and the total variance is

$$\mathbb{E}[\text{Var}(\varepsilon|x)] + \text{Var}(\mathbb{E}[\varepsilon|x]) = \overline{\sigma_{\text{model}}^2} + \sigma_N^2 + \text{Var}(u). \quad (33)$$

where $\text{Var}(u)$ can be estimated from the sampled population. The difference between the sampled variance s_ε^2 and the theoretical population variance σ_ε^2 resides in the computation of $\overline{\sigma_{\text{model}}^2}$. For σ_ε^2 , the model variance should cover approximately the residual by a factor of γ , which leads to the approximation $\sigma_{\text{model}}^2 = \gamma^2 u^2$. For s_ε^2 , the variance is provided by the sample evaluation as $\sigma_{\text{model}}^2 = (\sigma^h)^2$. Therefore, the corresponding variances are formulated as

$$\sigma_\varepsilon^2 = \overline{\gamma^2 u^2} + \sigma_N^2 + \text{Var}(u) \quad (34)$$

$$s_\varepsilon^2 = \overline{(\sigma^h)^2} + \sigma_N^2 + \text{Var}(u) \quad (35)$$

The distribution obtained in Equation 27 will be used to compute the likelihood function as in Equation 87. In this case, the first moment t_1 will be the mean of the full sample set and t_2 will be the mean value of the variances of the sample set. Additionally, instead of as a difference, the fit in t_2 is obtained through a ratio. The composed noise probability follows

$$\pi_\varepsilon(t(y) - t(f(\boldsymbol{\theta}))) = \pi_{t_1}(t_1(y) - t_1(f(\boldsymbol{\theta}))) \pi_{t_2}\left(\frac{t_2(f(\boldsymbol{\theta}))}{t_2(y)}\right) \quad (36)$$

For the first moment, the matching is expressed as

$$t_1(\mathbf{y}) - t_1(\mathbf{f}(\boldsymbol{\theta})) = \bar{\mathbf{y}} - \overline{\mathbf{f}(\boldsymbol{\theta})} = \bar{\mathbf{y}} - \overline{\boldsymbol{\mu}^h} = \overline{\mathbf{y} - \boldsymbol{\mu}^h} = \bar{\mathbf{u}}, \quad (37)$$

where $\bar{\mathbf{u}}$ represents the mean of the residuals and assuming that there is only one observation per individual sample. For the second moment, the variance in observations and predictions, including additive noise and the variance of the residuals, should be equal. The moment matching is done through a ratio between variances that should tend to 1 for perfect comparison:

$$\frac{t_2(\mathbf{f}(\boldsymbol{\theta}))}{t_2(\mathbf{y})} = \frac{\overline{(\sigma^h)^2} + \sigma_N^2 + \text{Var}(u)}{\overline{\gamma^2 u^2} + \sigma_N^2 + \text{Var}(u)} = \frac{s_\varepsilon^2}{\sigma_\varepsilon^2}. \quad (38)$$

As the sampled variance s_ε^2 is a sufficient statistic for the population variance σ_ε^2 given θ , the requirements from [Wilkinson \(2013\)](#) for a valid ABC probability distribution with noise hold for Equation 36.

This likelihood is derived from the normal structure of the prescribed measurement noise. According to Cochran's theorem ([Cochran \(1934\)](#)), the variables $\bar{\mathbf{u}}$ and s_ε^2 are independent random variables with known distributions, assuming that each sample is independent of the others. Specifically, we have $\bar{\mathbf{u}} \sim \mathcal{N}(\mu_\varepsilon, \sigma_\varepsilon/\sqrt{n})$ and $ns_\varepsilon^2/\sigma_\varepsilon^2 \sim \chi_{n-1}^2$, where χ_{n-1}^2 denotes a chi-square distribution with $n-1$ degrees of freedom. It is important to note that for large n , $s_\varepsilon^2 \sim \mathcal{N}(\sigma_\varepsilon^2, \sqrt{2/n}\sigma_\varepsilon^2)$. Although the assumption of independence among samples is typically not valid for computational models with correlated outputs, the correlation structure of the residuals is often unknown a priori. Thus, excluding it from consideration is a reasonable approach that provides a regularizing effect. While computing and incorporating correlation effects is beyond the scope of this paper, one potential strategy would involve including the covariance structure in the calculation of σ_ε^2 .

The likelihood function for the mean would directly be

$$\mathcal{L}_1^{\text{GMM}}(\theta) = \left(\frac{2\pi}{n}\sigma_\varepsilon^2\right)^{-\frac{1}{2}} \exp\left(-\frac{n\bar{\mathbf{u}}^2}{2\sigma_\varepsilon^2}\right). \quad (39)$$

In addition, the density function of a χ_{n-1}^2 distribution can be expressed as

$$f(x, n-1) = \frac{x^{\frac{n-1}{2}-1} \exp(-\frac{1}{2}x)}{2^{\frac{n-1}{2}} \Gamma(\frac{n-1}{2})}. \quad (40)$$

Hence, substituting $x = ns_\varepsilon^2/\sigma_\varepsilon^2$ in the χ_{n-1}^2 density function, it follows

$$\mathcal{L}_2^{\text{GMM}}(\theta) = \frac{1}{2^{\frac{n-1}{2}} \Gamma(\frac{n-1}{2})} \exp\left(-\frac{ns_\varepsilon^2}{2\sigma_\varepsilon^2}\right) \left(\frac{ns_\varepsilon^2}{\sigma_\varepsilon^2}\right)^{\frac{n-1}{2}-1} \quad (41)$$

where s_ε^2 and σ_ε^2 are obtained from Equations 34 and 35. The global moment-matching likelihood will be

$$\pi_\varepsilon^{\text{GMM}}(\theta) = \pi_\varepsilon(t(y) - t(f(\boldsymbol{\theta}))) = \mathcal{L}_1^{\text{GMM}}(\theta) \mathcal{L}_2^{\text{GMM}}(\theta) \quad (42)$$

and in logarithmic form,

$$\begin{aligned} \log \pi_\varepsilon^{\text{GMM}}(\theta) &= -\frac{1}{2} \log\left(\frac{2\pi}{n}\sigma_\varepsilon^2\right) - \frac{n\bar{\mathbf{u}}^2}{2\sigma_\varepsilon^2} \\ &\quad - \frac{n-1}{2} \log 2 - \log\left(\Gamma\left(\frac{n-1}{2}\right)\right) - \frac{ns_\varepsilon^2}{2\sigma_\varepsilon^2} + \left(\frac{n-1}{2} - 1\right) \log\left(\frac{ns_\varepsilon^2}{\sigma_\varepsilon^2}\right). \end{aligned} \quad (43)$$

2.5.4 Relative Global Moment-matching Likelihood with noise

The hypothesis that the absolute residuals ε follow the same normal distribution, which is necessary for the GMM likelihood, does not easily hold. A more reasonable assumption is that the relative residuals ε_r , defined as the absolute residuals scaled by the posterior-predictive standard deviation at that point, follow a common normal distribution, analogously as in GMM. Figure 2 is equivalent for RGMM, only using the relative residuals instead of the absolute ones. The model is then

$$\varepsilon_r(\boldsymbol{\theta}) = \frac{y(x) - f(\boldsymbol{\theta}, x)}{\sqrt{(\sigma^h)^2 + \sigma_N^2}}, \quad \varepsilon(\boldsymbol{\theta}) \sim \mathcal{N}(\mu_\varepsilon, \sigma_\varepsilon). \quad (44)$$

This interpretation is based on the belief that predictions scaled by its variance follow the same distribution. Therefore, predictions with wider variances admit larger residuals than those with smaller ones. This interpretation is comparable to the one made for independent normal Gaussian likelihoods, which is discussed in Section 2.5.5.

As in GMM, we impose $\mu_\varepsilon = 0$, and the mean to be fitted is now defined as

$$\bar{\varepsilon}_r = \overline{\left(\frac{u}{\sqrt{(\sigma^h)^2 + \sigma_N^2}} \right)}. \quad (45)$$

The total variance decomposition theorem is applied to obtain the sampled and population variances. The scaling factor $(\sigma_{\text{model}})^2$ is defined as $(\gamma u)^2 + \sigma_N^2$ for the population and $(\sigma^h)^2 + \sigma_N^2$ for the sample. Then,

$$\mathbb{E}[\varepsilon_r|x] = \frac{u}{\sqrt{(\sigma_{\text{model}})^2}} \quad (46)$$

$$\text{Var}(\varepsilon_r|x) = \frac{\sigma_{\text{model}}^2}{\sqrt{(\sigma^h)^2 + \sigma_N^2}} \quad (47)$$

$$\mathbb{E}[\text{Var}(\varepsilon_r|x)] = 1 \quad (48)$$

$$\text{Var}(\mathbb{E}[\varepsilon_r|x]) = \text{Var}\left(\frac{u}{\sqrt{(\sigma_{\text{model}})^2}}\right) \quad (49)$$

Adding the variance components, the obtained variance is

$$\text{Var}(\varepsilon_r) = \text{Var}\left(\frac{u}{\sqrt{(\sigma_{\text{model}})^2}}\right) + 1, \quad (50)$$

therefore

$$\sigma_{\varepsilon_r}^2 = \text{Var}\left(\frac{u}{\sqrt{(\gamma u)^2 + \sigma_N^2}}\right) + 1, \quad (51)$$

and

$$s_{\varepsilon_r}^2 = \text{Var}\left(\frac{u}{\sqrt{(\sigma^h)^2 + \sigma_N^2}}\right) + 1. \quad (52)$$

These values are directly substituted in Equations 39 to 43 to obtain the likelihood.

Notice that if σ_{model} is constant for every input value, then GMM and RGMM converge asymptotically to the same value up to a constant. In effect,

$$\bar{\varepsilon}_r = \overline{\left(\frac{u}{\sqrt{(\sigma^h)^2 + \sigma_N^2}} \right)} = \frac{\bar{u}}{\sqrt{(\sigma^h)^2 + \sigma_N^2}}, \quad (53)$$

$$\sigma_{\varepsilon_r}^2 = \text{Var}\left(\frac{u}{\sqrt{(\gamma u)^2 + \sigma_N^2}}\right) + 1 = \frac{\text{Var}(u)}{(\gamma u)^2 + \sigma_N^2} + 1 = \frac{\text{Var}(u) + (\gamma u)^2 + \sigma_N^2}{(\gamma u)^2 + \sigma_N^2} \quad (54)$$

and

$$s_{\varepsilon_r}^2 = \text{Var}\left(\frac{u}{\sqrt{(\sigma^h)^2 + \sigma_N^2}}\right) + 1 = \frac{\text{Var}(u)}{(\sigma^h)^2 + \sigma_N^2} + 1 = \frac{\text{Var}(u) + (\sigma^h)^2 + \sigma_N^2}{(\sigma^h)^2 + \sigma_N^2}, \quad (55)$$

which are asymptotically equivalent to Equations 37, 34 and 35, respectively, divided by a constant value, as $\sigma^h \rightarrow \gamma u$ by construction.

2.5.5 Independent normal likelihood

An alternative to moment-matching likelihoods is to adapt the classical Gaussian Likelihood to take into consideration the predictive variance. Based on the assumption that the residuals follow an independent normal distribution with mean zero and standard deviation of the predicted one, [Sargsyan et al. \(2015\)](#) propose

$$\mathcal{L}^{\text{IN}}(\boldsymbol{\theta}) = (2\pi)^{-\frac{N}{2}} \prod_{i=1}^N (\sigma_i^h)^{-1} e^{-\frac{(y_i - \mu_i^h)^2}{2(\sigma_i^h)^2}}. \quad (56)$$

If noise is accounted for in the variance computation, the likelihood must be modified accordingly, resulting in

$$\mathcal{L}^{\text{IN}}(\boldsymbol{\theta}) = (2\pi)^{-\frac{N}{2}} \prod_{i=1}^N \left(\sqrt{(\sigma_i^h)^2 + \sigma_N^2} \right)^{-1} e^{-\frac{(y_i - \mu_i^h)^2}{2((\sigma_i^h)^2 + \sigma_N^2)}}. \quad (57)$$

2.6 Discussion on likelihood selection

In this article, four likelihood functions are compared: ABC-Likelihood with noise (ABC), Global Moment-matching (GMM) likelihood, Relative Global Moment-matching (RGMM) and Independent Normal (IN) likelihood with noise. GMM and RGMM are new proposals developed in this work, while ABC and IN have been adapted from [Sargsyan et al. \(2019\)](#) to explicitly include noise. As a common feature, the four of them aim to match the mean and variance of the predicted output distribution with the data.

The likelihood models present substantial differences in their behaviour that influence their choice over the others depending on the characteristics of the dataset:

- **Number of parameters:** ABC requires prescribing γ and ϵ , while GMM and RGMM only require γ and IN none. As already mentioned, the choice of ϵ is not trivial for datasets with prescribed noise and can largely impact the results. Additionally, the choice of γ corresponds to previous beliefs on the expected predicted distribution. In particular, a value of $\gamma = \sqrt{\frac{\pi}{2}}$ is expected for ABC and $\gamma = 1.0$ for the others.
- **Noise misspecification:** As shown in Appendix C, ABC is very sensitive to the specification of the noise amplitude, which can lead the parameter updating procedure to values of $\boldsymbol{\theta}$ further from the expected ones. The misspecification of the prescribed noise generally leads to larger acceptance ratios and wider posterior distribution of $\boldsymbol{\theta}$ for GMM, RGMM and IN.
- **Assumptions of normality:** The four likelihoods considered suppose different distributions of the residuals while still keeping the assumption of normality. ABC fits exactly the moments under the consideration of Gaussian noise. GMM impose the condition that all the residuals are characterized by the same Gaussian distribution, which may not be reasonable. RGMM assume that the relative errors between observations and predicted distribution follow a common Gaussian distribution. Finally, IN assumes independent normal distributions for each observation. Depending on the application case, some of these assumptions may not hold.
- **Inferred posterior distribution:** By construction, ABC aims to match the statistical moments exactly up to a tolerance, which will lead to narrow inferred posterior distributions of $\boldsymbol{\theta}$ compared to GMM, RGMM and IN. In particular, larger predicted variances imply more samples needed for the convergence of the chain ([Schälte and Hasenauer \(2020\)](#)). Additionally, the formulation of $\mathcal{L}_2(\boldsymbol{\theta})$ for GMM and RGMM produces a flatter likelihood function in the direction of the variance-governing parameters, which further hinders the convergence for those parameters.
- **Observations out of the predictive range:** If the observations cannot be replicated by the computational model independently of the choice in the parameters, then embedded approaches lead to suboptimal results. RGMM and IN are expected to be the most impacted if those values are at points with low predictive variance. However, the regularizing effect of considering the whole dataset in RGMM and GMM for the goodness of fit instead of fitting every point, as in IN or ABC, should reduce the impact of these observations if they are not predominant in the dataset.
- **Fit to exact observations:** As pointed out in [Sargsyan et al. \(2015\)](#), marginalizing formulations such as IN would lead to wrong results if σ_i^h for a given observation i where the variance is significantly smaller than for the others. In those cases, such observation will be overfitted by reducing the residual to the minimum to the detriment of the other observation points with larger variances. The presence of prescribed noise reduces this occurrence. RGMM mitigates the possibility of overfitting to one observation through the inclusion of $\text{Var}\left(u/\sqrt{(\sigma_{\text{model}})^2}\right)$ in the likelihood computation of Equation 50, which penalizes increasing the variance between samples. The presence of a prescribed noise also reduces this effect in IN and RGMM likelihoods, as all observations will have at least variance σ_N . For an analysis on this phenomena, refer to [Sargsyan et al. \(2015\)](#).

2.7 Pushed-forward prediction of Quantities of Interest

The solution of the inverse problem provides the joint posterior distribution $\pi(\boldsymbol{\theta}^m, \boldsymbol{\theta}^b | \mathbf{y})$. The predicted response $\mathbf{f}_P(\boldsymbol{\theta}^m, \boldsymbol{\theta}^b, \mathbf{x} | \mathbf{y})$ is to be computed. To do so, the posterior distribution of the latent parameters should be propagated through the forward model. The response generated by \mathbf{f} is stochastic, which increases the complexity of the propagation. A common approach (Huan et al. (2017); Sargsyan et al. (2019)) is to use an estimator $\hat{\boldsymbol{\theta}}$ of the latent parameters, typically a maximum-a-posteriori (MAP) one. The predicted response is then

$$\mathbf{f}_P(\hat{\boldsymbol{\theta}}^m, \hat{\boldsymbol{\theta}}^b, \mathbf{x} | \mathbf{y}) = \mathbf{f}(\hat{\boldsymbol{\theta}}^m, \hat{\boldsymbol{\theta}}^b, \mathbf{x}). \quad (58)$$

Due to the embedding, \mathbf{f}_P generates a stochastic response that usually does not have a tractable form. Therefore, either the procedure specified in Section 2.3 or Monte-Carlo methods can be used to obtain the moments of the approximated predicted response $\boldsymbol{\mu}_P^h$ and $\boldsymbol{\sigma}_P^h$. One of the main characteristics of \mathbf{f}_P as shown by Sargsyan et al. (2019) is that the variance of the response does not reduce to zero for large sample sets, preserving the variance due to the dataset and the model discrepancy.

A special case is the propagation of the uncertainty obtained for the inferred parameters through the embedding and solution of the inverse problem to other Quantities of Interest (QoI) that did not take part in the inference procedure. The function \mathbf{g} that represents the QoI based on the inferred parameters is defined analogously to \mathbf{f} following Equation 4. Then, the posterior distribution must be pushed through \mathbf{g} in the same way as for \mathbf{f}_P . The predicted QoI will include the uncertainty expressed through the inferred embedded latent variables.

Nevertheless, using an estimator for $\boldsymbol{\theta}$ presents several drawbacks. First, $\hat{\boldsymbol{\theta}}$ are pointwise estimators despite generating a predictive distribution $\hat{\mathbf{f}}_P$. The information they provide is limited, losing the structure and potential correlations that are present in the joint posterior distribution of the latent parameters. Pointwise estimators fail as well in multimodal distributions to represent other local maximums apart from the optimum, which may be relevant for the QoI. Additionally the distribution obtained from $\mathbf{f}_P(\hat{\boldsymbol{\theta}}^m, \hat{\boldsymbol{\theta}}^b, \mathbf{x} | \mathbf{y})$ only preserves the uncertainty provided by the model bias parameters $\boldsymbol{\theta}^b$, disregarding the variance obtained through the inference procedure, which leads to potentially overconfident predictions.

As an alternative, in this article we propose a full propagation of the posterior distributions of the latent parameters as

$$\mathbf{f}_P(\boldsymbol{\theta}^m, \boldsymbol{\theta}^b, \mathbf{x} | \mathbf{y}) = \mathbf{f}(\boldsymbol{\theta}^m, \boldsymbol{\theta}^b, \mathbf{x}), \quad (59)$$

or $\mathbf{g}(\boldsymbol{\theta}^m, \boldsymbol{\theta}^b, \mathbf{x} | \mathbf{y})$ for QoIs other than the predictions. By propagating the joint posterior distribution, the full information obtained during the inference procedure is preserved. This allows not only obtaining a predictive posterior distribution \mathbf{f}_P or \mathbf{g} , but also perform inference on its parameters, providing additional insight on its reliability. For example, it is possible to obtain the pushed-posterior distribution of $\boldsymbol{\mu}_P^h$, where propagating the estimators would have only provided a point value. Two main challenges arise with this approach: the increasing number of evaluations of \mathbf{f} or \mathbf{g} and the composition of stochastic variables. First, the additional evaluations come from the need of sampling the joint posterior distribution of the latent parameters, which implies evaluating \mathbf{f} or \mathbf{g} each of the samples. These samples of $\boldsymbol{\theta}$ define random variables as inputs, therefore \mathbf{f} and \mathbf{g} necessarily generate a stochastic response. To reduce the number of evaluations of \mathbf{f} and \mathbf{g} , a PCE approximation of the response or the use of surrogate models are available. Additionally, the composition of stochastic variables requires explicit treatment. If the QoI is a property of the pushed-posterior distribution, such as $\boldsymbol{\mu}_P^h$ and $\boldsymbol{\sigma}_P^h$, then the results are directly posterior distributions that can be analyzed with statistical inference tools. However, if the QoI is the value of a given realization of \mathbf{f}_P or \mathbf{g} , the posterior distribution must account for the variability in the sampled $\boldsymbol{\theta}$ and the variance from the predicted distribution itself. In this paper, this situation will be solved by sampling from the pushed-posterior distributions $\mathbf{f}_P(\boldsymbol{\theta}_i^m, \boldsymbol{\theta}_i^b, \mathbf{x} | \mathbf{y})$ or $\mathbf{g}(\boldsymbol{\theta}_i^m, \boldsymbol{\theta}_i^b, \mathbf{x} | \mathbf{y})$ for every $(\boldsymbol{\theta}_i^m, \boldsymbol{\theta}_i^b)$ in n_P samples of $\boldsymbol{\theta}$ and analyzing the resulting dataset.

The QoIs obtained from the computational model are observed by *virtual* sensors (Andrés Arcones et al. (2023)). In contrast with *real* sensors that are installed in the physical system, virtual sensors observe values provided by the computational model. They are not limited to observable quantities as the real sensors, but can represent any QoI. For example, virtual sensors may observe the value of the model prediction \mathbf{f} , but also the mean $\boldsymbol{\mu}_P^h$ and standard deviation $\boldsymbol{\sigma}_P^h$ of the predictive response or the limits of the confidence interval for a given QoI calculated through \mathbf{g} . Quantifying the uncertainty in the output of virtual sensors is key for an assessment of the reliability of the predictions of QoIs.

3 Applications

3.1 Simple example

This example aims to test the behaviour of the different likelihood formulations under known conditions. The same model is used to generate the dataset and to compute the predictions:

$$\mathbf{y} = \boldsymbol{\theta} \mathbf{x} + \boldsymbol{\varepsilon}_N \quad (60)$$

where $x \in [0, 1]$ is the input variable, y is the output variable, θ is the slope parameter to be inferred and ε_N is a white noise perturbation. The generator aims to provide a sample of observations generated by the computational model given $\theta \sim \mathcal{N}(4.0, 1.0)$. The observations \mathbf{y} are then generated by evaluating Equation 60 with a random value of θ from the aforementioned distribution for each entry the input vector \mathbf{x} and adding a random perturbation of $\varepsilon_N \sim \mathcal{N}(0, \sigma_{\text{true}}^2)$ with $\sigma_{\text{true}} = 0.01$. If not specified for a particular analysis, \mathbf{x} is composed of 120 equidistant samples covering the range $[0.4, 1.0]$. An example of a generated dataset is presented in Figure 3

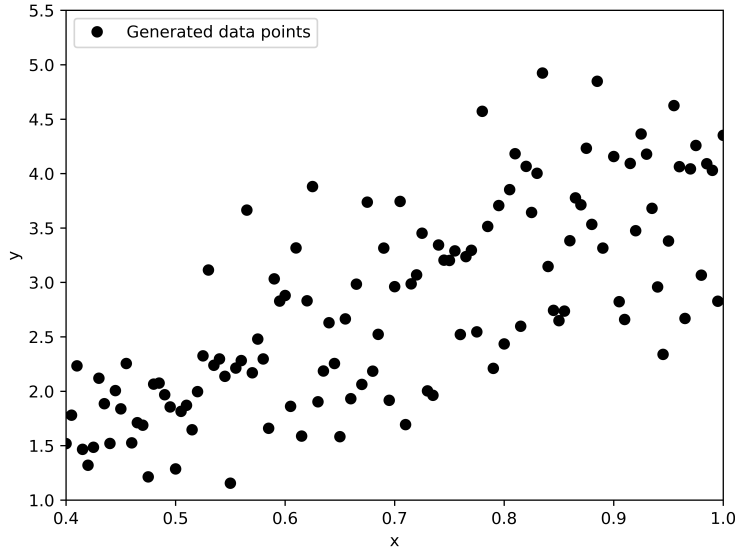


Figure 3: Generated dataset of the simple example for 120 data points

The extended variable θ^* with the embedding is defined as

$$\theta^* = t + \delta_b, \quad \delta_b \sim \mathcal{N}(0, \sigma_b^2) \quad (61)$$

where t would correspond to the original latent variable and σ_b is the new additional latent variable associated with the bias. This is equivalent to imposing $\theta^* \sim \mathcal{N}(t, \sigma_b^2)$ and using θ^* instead of θ in Equation 60. As the forward model is a linear function and θ^* follows a normal distribution, a closed-form expression of \mathbf{f} is available in this case and can be formulated as

$$\mathbf{f}(t, \sigma_b, \mathbf{x}) = \theta^* \mathbf{x} + \varepsilon_N \Rightarrow f(t, \sigma_b, x_i) \sim \mathcal{N}(tx_i, (\sigma_b^2 x_i^2 + \sigma_N^2)) \quad \forall i = 1, 2, \dots, n. \quad (62)$$

The existence of a closed-form solution provides analytical expressions for the statistical moments of $f(t, \sigma_b, x_i)$ for every x_i in \mathbf{x} and sampled t and σ_b . Nevertheless, a PCE approximation of the forward model response is built in the interest of testing the whole methodology developed in Section 2. As the response is a linear function and the input is normal, a first degree PCE with Hermite polynomials and two Gauss points is exact and the approximation error tends to zero. The statistical moments of the computed response $\boldsymbol{\mu}^h$ and $\boldsymbol{\sigma}^h$, which are necessary to evaluate the likelihood functions in the inference procedure, are then obtained from Equations 15 and 16.

To obtain the posterior probability $\pi(t, \sigma_b | \mathbf{y})$, an MCMC algorithm with the tested likelihood models is applied to the generated dataset \mathbf{y} . The algorithm is run until convergence with a threshold of $\widehat{ESS} = 837$ or a maximum of 3500 MCMC samples.

The prior distributions for the parameters are $\pi(t) \sim \mathcal{N}(4.5, 0.5^2)$ and $\pi(\sigma_b) \sim \mathcal{LN}(-1, 0.5)$. The prior for σ_b is chosen as a log-normal distribution to ensure the positivity. The chosen parameters lead to $\sigma_b \in [e^{-1.5}, e^{-0.5}]$ in the range of one standard deviation. Additionally, $\pi(t)$ is truncated to the region $[3.0, 5.0]$ to reflect the belief that the slope parameter can only exist in that range. These prior distributions are informative enough to guide the inference procedure while still covering the expected latent variable space reasonably well.

The pair plots for the posterior $\pi(t, \sigma_b | \mathbf{y})$ from applying the MCMC algorithm with each likelihood formulation and the posterior predictive for its mean are shown in Figure 4. Each likelihood leads to converged values close to the true generating parameters $t = 4.0$ $\sigma_b = 1.0$. The results are presented in Table 1. The different convergence plots for this dataset are presented in Figure

The different likelihood models provide posterior distributions centered around the same values of the latent parameters. The distribution provided by the ABC likelihood presents significantly less variance than the others.

Table 1: Posterior results for the linear model and different likelihoods

| Likelihood | t | | | σ_b | | |
|------------|------|------|-----------|------------|------|-----------|
| | Mean | Std | \hat{R} | Mean | Std | \hat{R} |
| ABC | 4.00 | 0.00 | 858 | 0.98 | 0.00 | 947 |
| GMM | 4.05 | 0.11 | 1061 | 0.80 | 0.13 | 851 |
| RGMM | 4.05 | 0.12 | 900 | 0.94 | 0.13 | 1061 |
| IN | 4.03 | 0.08 | 1204 | 0.90 | 0.06 | 850 |

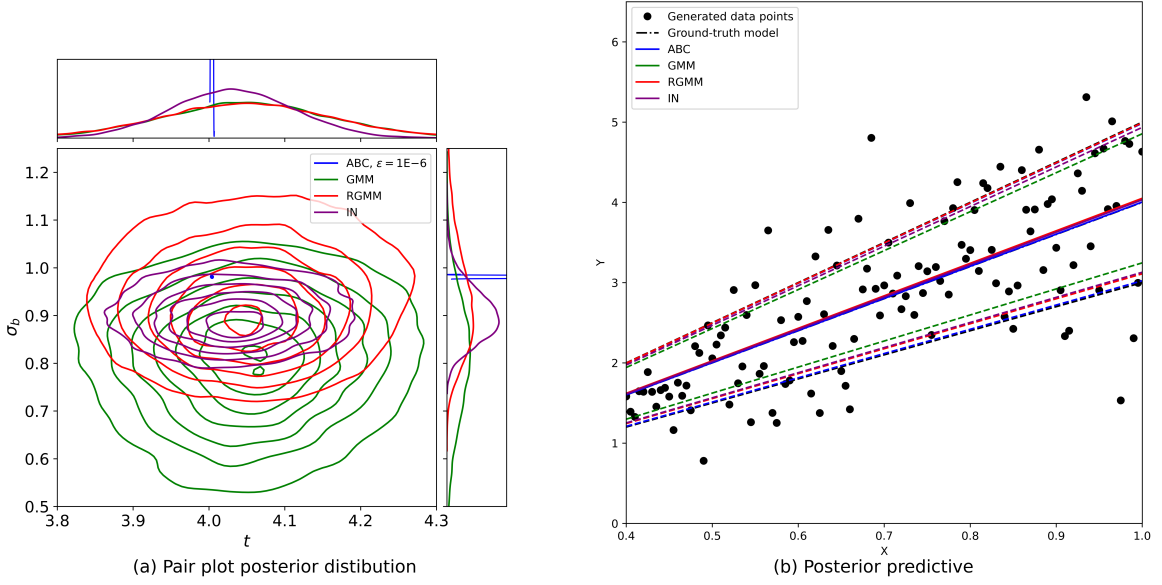


Figure 4: Comparison for the converged solution of linear example. (a) Pair plot of the posterior distribution for t and σ_b . (b) Predictive distribution from the mean of the posterior distributions of t and σ_b

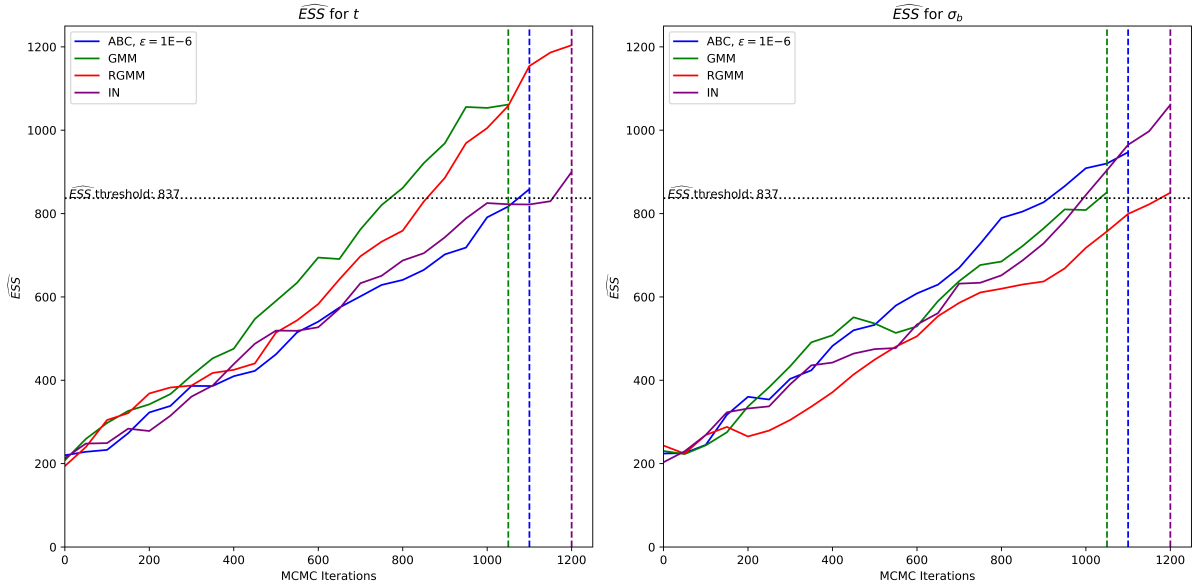


Figure 5: Estimated sample size (ESS) for the simple example over the MCMC iterations

This is due to the fitting of σ_b being exact up to ϵ as a difference, while the other likelihoods have larger acceptance probabilities for the values of σ_b . GMM presents the larger variance due to the conditions of the likelihood not being necessarily fulfilled. There is no significant difference in the convergence speed for this particular dataset.

Four QoI are evaluated for $x = 1.0$: the output y , the mean of the predictive distribution μ_P^b , the standard

deviation σ_P^h and the z-value of $y(1.0)$. The output y is directly the pushed-forward prediction $f_P = f(t, \sigma_b, x)$, as described in Section 2.7. The other QoIs are calculated for each sample of the posterior distribution of the parameters. In particular, the z-value $|Z| = \left| \frac{\mu_P^h - y(1.0)}{\sigma_P^h} \right|$ can be used for testing the hypothesis H_1 : the value $y(1.0)$ has not been generated by a normal distribution $\mathcal{N}(\mu_P^h, \sigma_P^h)$ against the null hypothesis H_0 . The critical threshold of $|Z|$ for a confidence level of 95% is 1.96, allowing to reject H_0 if the value of $|Z|$ is significantly larger. For comparison, the equivalent QoIs obtained with the MAP estimator of t and σ_b are calculated as well. The results are plotted in Figure 6.

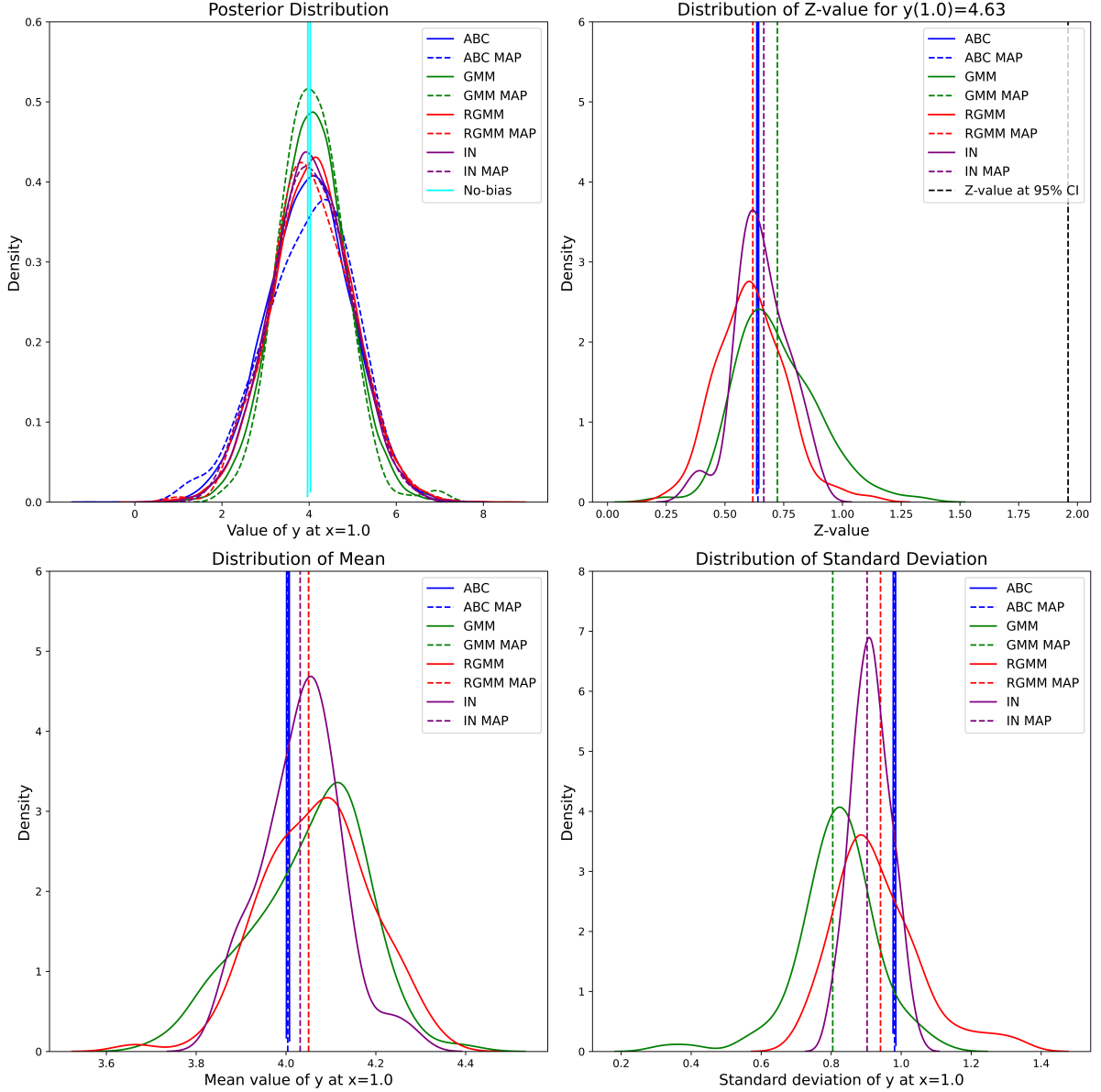


Figure 6: Analysis of Quantities of Interest by propagating the posterior distribution of t and σ_b for the simple example

The obtained propagated distribution is comparable for all likelihoods, either using an estimator of the posterior or sampling from the distribution. The distributions for μ_P^h and σ_P^h reflect the same conclusions from the pair plot representation. This is due to the linear nature of the system, which propagates directly the posterior distribution of the parameters, as t controls μ_P^h and σ_b , σ_P^h . The z-values are below 1.96 for all likelihoods, failing to reject H_0 , meaning it is plausible that the data point $y(1.0) = 4.63$ was generated by the corresponding posterior distribution. In comparison, if the no bias had been introduced and the posterior only considered the prescribed noise as source of variance, the corresponding z-value would have been 63, which allows to reject H_0 , inferring that the data point could not have been generated by the prediction. It is noted that if only the estimators where propagated, it would not be possible to generate distributions for three of the QoI, and the values indicated in

Figure 6 as dashed lines would be taken as the predicted ones.

3.1.1 Dataset dependency analysis

While the obtained results provide insight into the properties of the different likelihoods for this case, it is necessary to compare them with several datasets generated analogously. The described procedure was repeated for 20 datasets with different random seeds for the data generation. The summary of results is presented in Figure 7.

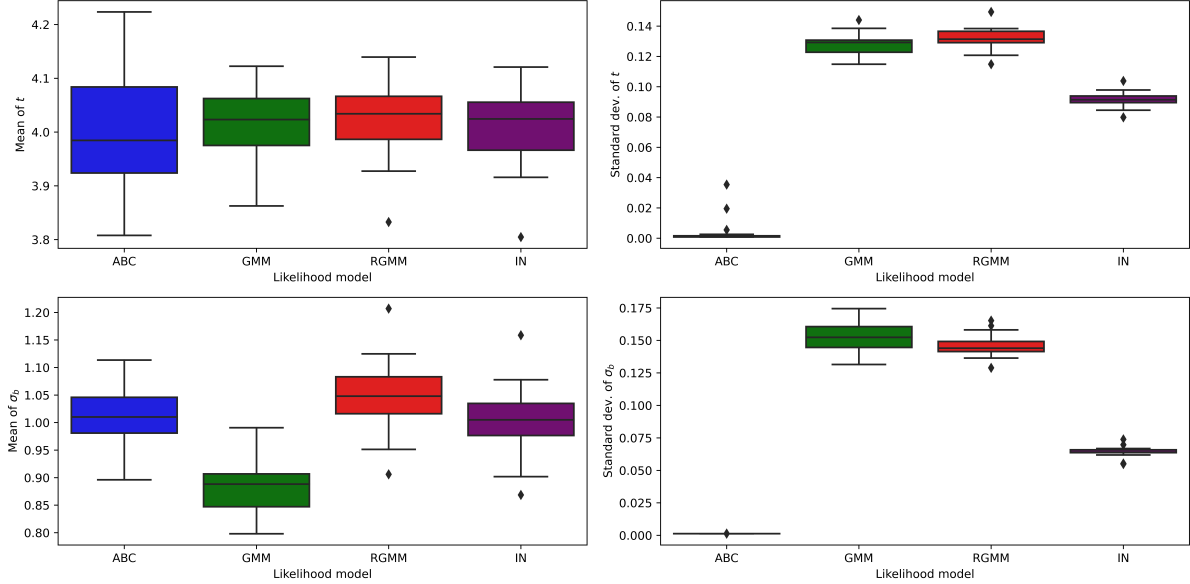


Figure 7: Box plots for the latent parameters of the embedded model with different likelihoods. Mean and standard deviation of the posterior distribution after 1000 MCMC evaluations with 10 walkers and 200 burn-in steps. Mean (top left) and standard deviation (top right) for the slope variable t and mean (bottom left) and standard deviation (bottom right) of the bias scale parameter σ_b

As it can be observed, the mean value of t using ABC varies the most from dataset to dataset, followed then by GMM and finally RGMM and IN being mostly equivalent. Coincidentally, ABC presents the smallest variance in the posterior. Due to the limited dataset, ABC tends to overfit to the available points, which may have a slight, as it aims to fit the moments exactly. This explains as well the fast convergence of ABC in comparison with the rest, as fewer samples with low likelihood are accepted. When comparing the bias results, the means for ABC, RGMM and IN are comparable, following the same pattern in their respective standard deviations. The only difference comes from GMM, for which the limited dataset does not hold the assumptions required for this likelihood, as in the case previously analyzed.

An analysis on the speed of convergence is presented in Figure 8. The ABC likelihood presents a larger variance in the number of MCMC samples to converge, with a significant amount of outliers for the \widehat{ESS} of σ_b . Due to the exact matching of the statistical moments, the ABC likelihood may require longer chains in the MCMC algorithm. It must be noted that this can be controlled by the value of the tolerance parameter ε . The other likelihood models present comparable convergence behaviour with each other.

3.1.2 Noise influence analysis

It has been proved in Section 2 and Appendix C that the ABC likelihood is very sensitive to the prescribed additive noise σ_N , and in particular to its misspecification. We repeat the basic experiment, but with 20 different values for the prescribed σ_N between 0.001 and 10.0. The posterior predictive results are presented in Figure 10 and the compared influence of the noise in 10. As expected, the ABC likelihood is the most affected by the noise misspecification. This is the most noticeable for those values of σ_N larger than 1.0. For $\sigma_N < 0.01$, the prescribed noise underestimates the one used in the generative problem, and the additional variability is absorbed by the bias estimation. However, due to the difference in scale, this is not observable in the results. For values $0.01 < \sigma_N$, the noise is overestimated at least for some data samples, which would lead to a smaller contribution of σ_i^h to the predictive variance to be fixed at those points. In particular, for $\sigma_N > 0.4$, the prescribed noise at some points is larger than the variance of the data generator. This results in drastic changes in the inferred parameters. From $\sigma_N > 1.0$, all the samples in the dataset have an overestimated variance. The effect of this overestimation on the latent parameter t can be observed specifically for ABC, as it tries to fit the variance and

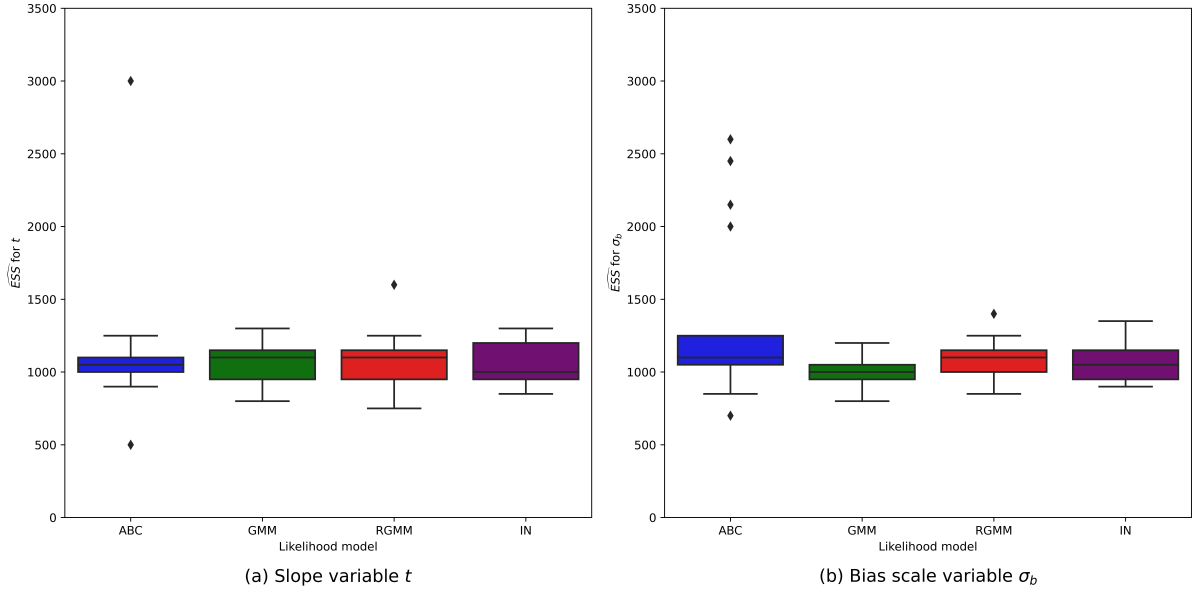


Figure 8: Boxplot of required number of MCMC samples until reaching the threshold $\widehat{ESS} = 837$ for the simple example.

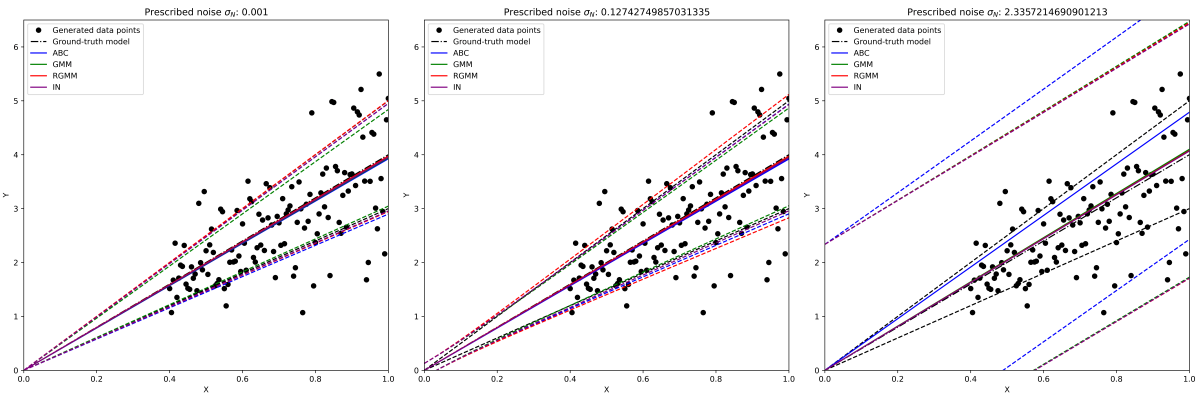


Figure 9: Posterior prediction comparison for noise value σ_N of 0.001, e^{-2} and $e^{0.85}$, chosen using a logarithmic rule.

the mean perfectly. The other likelihoods also converge to progressively worse values for t as the noise increases due to the larger dispersion, but the effect is less severe than for ABC. For low values of overestimated σ_N , large relative errors are generated, which makes RGMM slow convergence in the bias parameter and leads to a very wide posterior distribution with an overestimated mean. For larger values of σ_N , RGMM follows the same trend as the other likelihoods, which compensates it through a combination of low bias and increasing values of t with wider posteriors due to the additional noise.

3.1.3 Offset influence analysis

Another influential factor in the choice of the likelihood formulation is the existence of data points that cannot be replicated by the response function. This can be simulated by including an additive offset Δy to the generator as

$$y = \theta x + \Delta y + \varepsilon_N \quad (63)$$

while keeping the original computational model. This case is relevant, for example, for non-stationary problems that depend on initial conditions which may introduce such an offset. An offset in the range between 0.0 and 1.0 is tested. The posterior predictive results are presented in Figure 11 and the influence comparison in Figure 12. Increasing offset values lead to higher values for t to try to fit the observed points. At the same time, this leads to the need for larger variances to cover the dataset. This effect is more pronounced in RGMM and IN as the offset impacts in particular values with smaller σ_i^h , that need larger changes in t and σ_b to cover the new dataset, and coincidentally are those with the largest weight in those likelihood models.

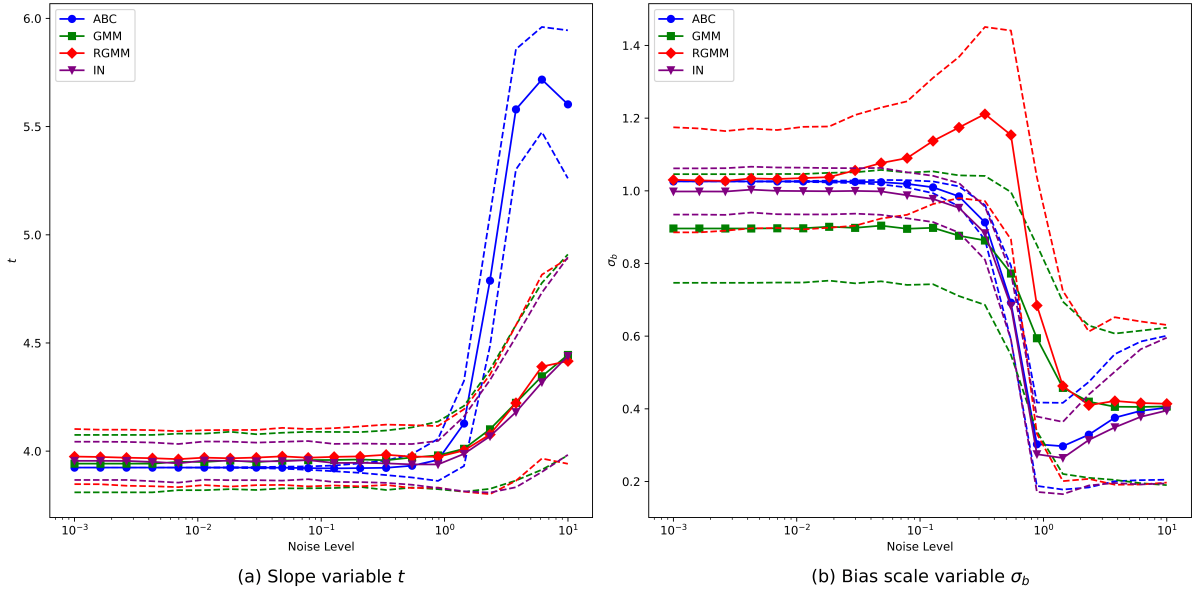


Figure 10: Influence of prescribed noise value σ_N for (a) slope variable t and (b) bias scale variable σ_b

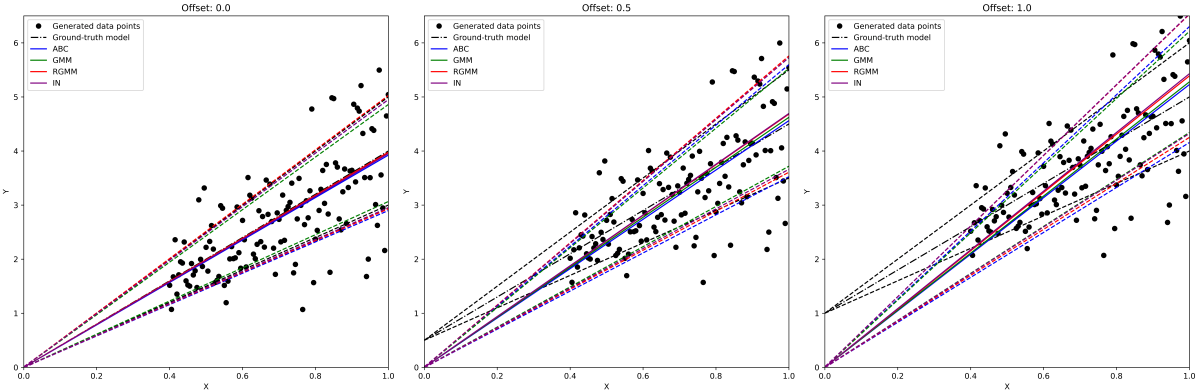


Figure 11: Posterior prediction comparison for offset values of 0.0, 0.5 and 1.0

3.1.4 Outlier influence analysis

An alternative situation in which an offset is present is if it only affects a given subset of data points, creating a group of outliers that influence the inference. In this case, Equation 63 is modified to only affect a subset of samples such that

$$y = \begin{cases} \theta x + \varepsilon_N & \text{if } x \in [0.4, 0.6] \cup (0.7, 1.0] \\ \theta x - \Delta y + \varepsilon_N & \text{if } x \in [0.6, 0.7] \end{cases}. \quad (64)$$

The offset ranges from 0.0 to 2.0 in 21 samples. The posterior predictive results are presented in Figure 13 and the comparison in 14.

In this case, ABC is the most affected in comparison with the other likelihood models. The outliers can be represented by the predicted response, but the fitting of every point with equal weight provokes larger deviations in ABC. Nevertheless, if the outliers are located at data points with low predicted variance, it is expected that RGMM and IN show a larger influence.

3.2 Application case: transient thermal simulation of reinforced concrete

The second application case consists of a transient thermal 2D simulation of the section of a reinforced concrete cylinder with constant external temperature. Due to symmetry and under the assumption of an infinitely long cylinder, such a system can be modeled as a 2D square section with adiabatic boundary conditions at the top, bottom and left-hand sides and constant temperature at the right-hand side. The Figure 15 shows a schematic representation of the case. The adiabatic conditions represent the periodic nature of the reinforcement for the sides and an isolation layer for the back. The system is reduced to from a 3D cube to the 2D section assuming

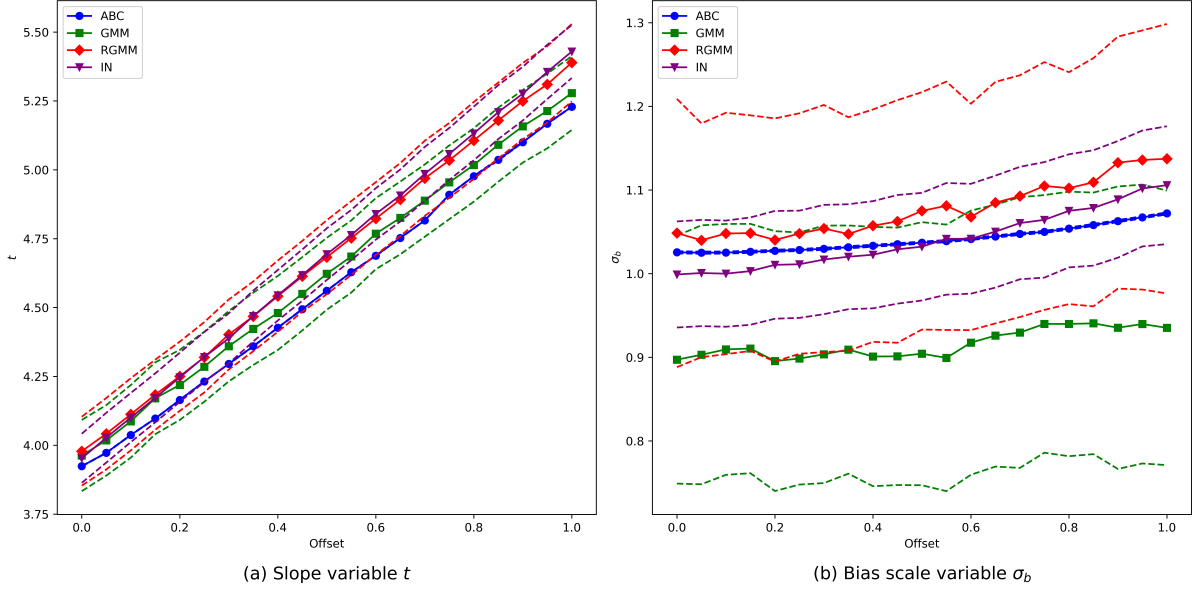


Figure 12: Influence of prescribed offset Δy for (a) slope variable t and (b) bias scale variable σ_b

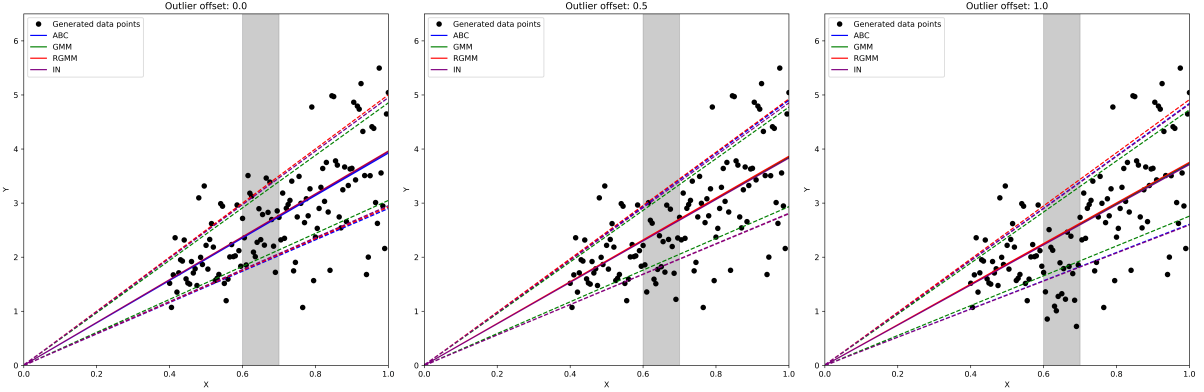


Figure 13: Posterior prediction comparison for outlier's offset values of 0.0, -0.5 and -1.0. The zones with outliers are shaded in grey

constant properties in X direction. The diagrams in Figure 16 represent the generative and forward models for this application case. The objective is to obtain the total cumulative heat $Q_{\text{obj}}(t)$ that passes through the middle line of the section at a given time. The heat flux through the structure is typically used to evaluate its energy efficiency and isolation properties under an external thermal load, as in Shen et al. (2021) and Wang et al. (2021).

The transient thermal system follows the heat equation for temperature T

$$\rho c_p \frac{\partial T}{\partial t} - \nabla \cdot (k \nabla T) = \dot{q}_V \quad (65)$$

where ρ is the density of the material, c_p its heat capacity, k its conductivity and \dot{q}_V is the volumetric heat flux in the system. There exists a linear relationship between k and c_p for a given ρ which is the diffusivity $\alpha = k/(\rho c_p)$, which requires correcting the heat component as $\dot{q}_V/(\rho c_p)$. The heat flux vector field at a given time t is defined as

$$\mathbf{q}(t) = -k \nabla T, \quad (66)$$

where k is calculated for a certain ρ , c_p and α , and the heat flux through the midline is obtained by integrating the normal heat flux field over the facet S as

$$\dot{Q}_{\text{obj}}(t) = \int \dot{\mathbf{q}}(t) \cdot \mathbf{n} dS. \quad (67)$$

The cumulative heat at time t_n is obtained by integrating $\dot{Q}_{\text{obj}}(t)$ over time, which in this case will be done using

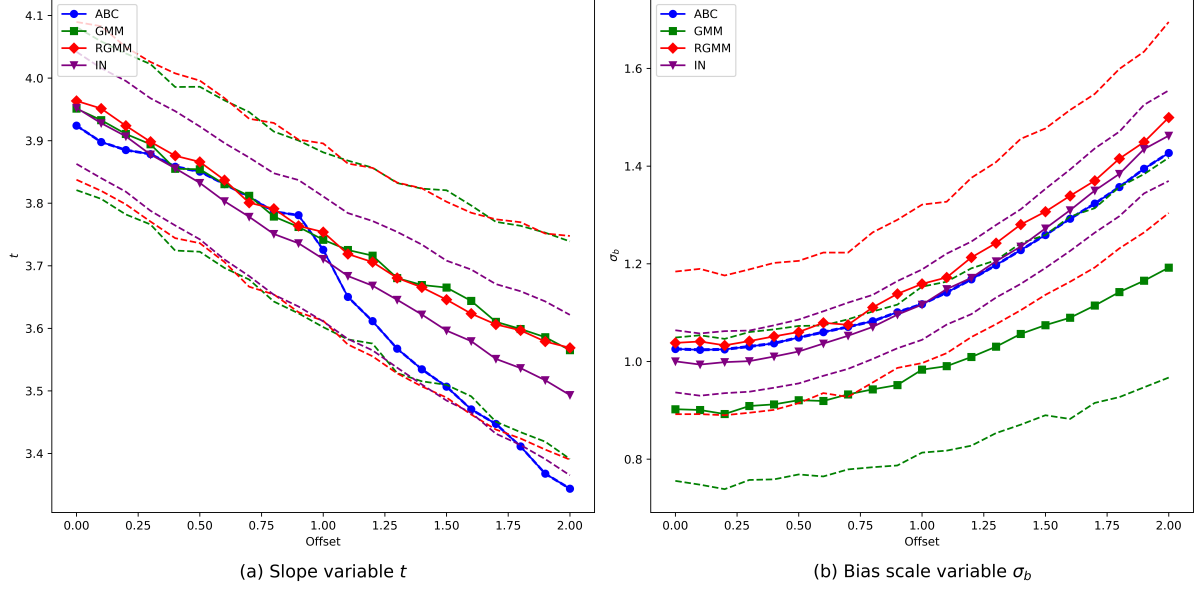


Figure 14: Influence of outlier data magnitude for (a) slope variable t and (b) bias scale variable σ_b

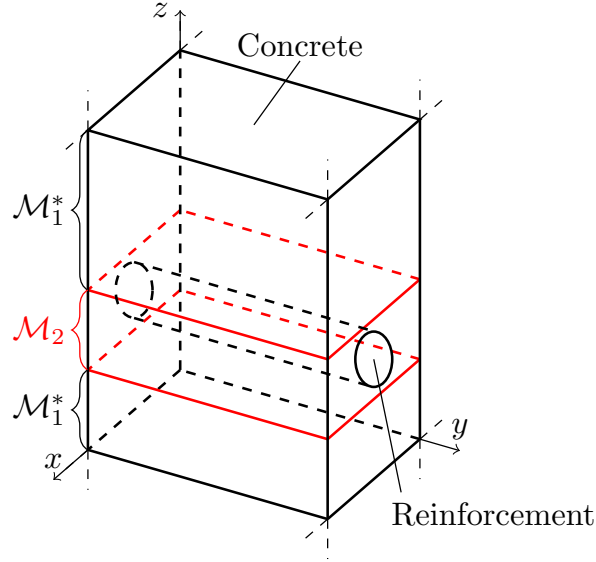


Figure 15: Schematic diagram of the heat example case

a trapezoidal rule as

$$Q_{\text{obj}}(t_n) = \int_{t_0}^{t_n} \dot{Q}_{\text{obj}}(t) dt \approx \sum_{i=0}^{n-1} \frac{\Delta t_i}{2} [\dot{Q}_{\text{obj}}(t_i) + \dot{Q}_{\text{obj}}(t_{i+1})], \quad (68)$$

where t_i are the discretized time points and Δt_i is the interval between two consecutive times t_i and t_{i+1} .

Altogether, the system's geometry, material properties ρ , c_p and k and its thermal and initial boundary conditions are required to calculate $\dot{Q}_{\text{obj}}(t)$. In this case, the squared slab has a length of 0.4 m in each direction, with adiabatic boundary conditions in three sides ($\dot{Q} = 0$ W) and fixed external temperature $T_{\text{ext}} = 303$ K. The initial temperature at all points of the system is $T(t = 0) = 273$ K and we assume a known density for the concrete of 2300 kg/m^3 . The diffusivity value α determines the thermal behaviour and must be estimated from the observations.

For the parameter estimation, two material models are implemented: an isotropic one \mathcal{M}_1 for the forward model and a biphasic one $\mathcal{M}_1 + \mathcal{M}_2$ representing the real reinforced system for the generative model. \mathcal{M}_1 is based on the assumption that the whole system shares the same material properties. Therefore, $\mathcal{M}_1 = \{\rho = 2300 \text{ kg/m}^3, c_p = 900 \text{ J/(kg} \cdot \text{K)}, \alpha\}$ with α to be inferred. The values of ρ and c_p have been chosen to reflect concrete properties at $T = 293$ K according to EN 1992-1-2:2004 ([European Committee for Standardization](#)

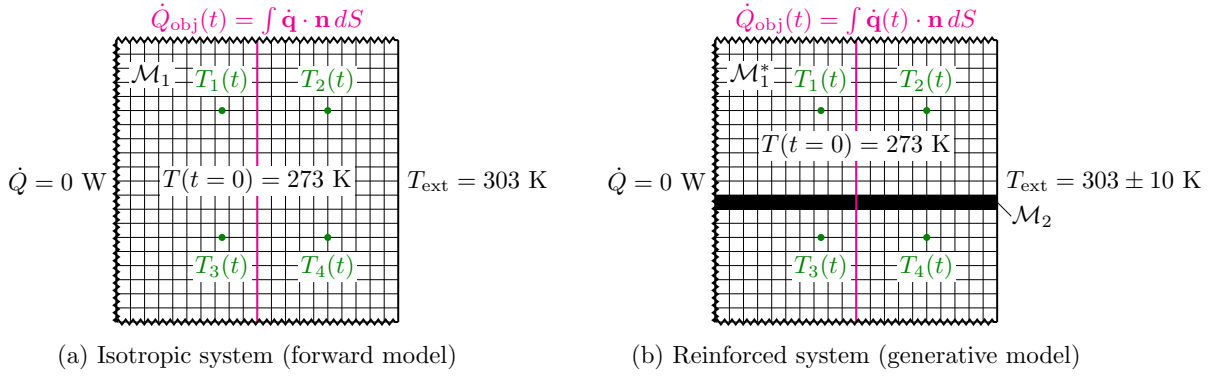


Figure 16: Diagrams of the systems modeled in the thermal example. (a) System with isotropic material properties \mathcal{M}_1 and (b) system with a band with modified material properties \mathcal{M}_2 that represent a reinforcement bar in that region. The temperature sensors $T_i(t)$ for $i = 1, 2, 3, 4$ act as *real* sensors and are used for updating the material parameters of \mathcal{M}_1 . The *virtual* sensor $\dot{Q}_{\text{obj}}(t)$ predicts the heat through the midline of the system obtained by integrating its normal heat-flow obtained from the gradient of the temperature field. The Quantity of Interest $\dot{Q}_{\text{obj}}(t)$ is the cumulative heat through the middle line at a given t .

(2004)). A reference value for the conductivity from these conditions is $k = 2.0 \text{ W}/(\text{m}\cdot\text{K})$. This simplified model responds to the situation where the location of the reinforcement bars is not known beforehand or their effect on the simulation is disregarded.

The biphasic model $\mathcal{M}_1^* + \mathcal{M}_2$ is used to generate the “real” observations required for the parameter estimation. The system is divided into two materials, \mathcal{M}_1^* for the concrete and \mathcal{M}_2 for the reinforcement. The properties for the concrete are taken from EN 1992-1-2:2004 (European Committee for Standardization (2004)) as $\mathcal{M}_1^* = \{\rho = 2300 \text{ kg}/\text{m}^3, c_p = 900 \text{ J}/(\text{kg}\cdot\text{K}), \alpha = 9.66 \cdot 10^{-7} \text{ m}^2/\text{s}\}$. To obtain \mathcal{M}_2 , a mix of material properties from the steel of the reinforcement and the concrete part must be considered. The region denoted for \mathcal{M}_2 has a height of 0.02 m located between $Y=0.16 \text{ m}$ and $Y=0.18 \text{ m}$, which, assuming the same depth, leads to a total surface perpendicular to the reinforcement of 0.0004 m^2 . Using a standard bar diameter of 12 mm, the fractional volumes for concrete and steel are

$$f_{\text{steel}} = \frac{V_{\text{steel}}}{V_{\text{total}}} = \frac{A_{\text{steel}} \cdot L}{A_{\text{total}} \cdot L} = \frac{0.012^2 \cdot 0.25 \cdot \pi}{0.0004} = 0.283 \quad (69)$$

and

$$f_{\text{concrete}} = 1 - f_{\text{steel}} = 0.717. \quad (70)$$

The material parameters M_i of \mathcal{M}_2 are then calculated as

$$M_i = f_{\text{steel}} M_{\text{steel}} + f_{\text{concrete}} M_{\text{concrete}}, \quad (71)$$

which for $\mathcal{M}_{\text{steel}} = \{\rho = 7850 \text{ kg}/\text{m}^3, c_p = 440 \text{ J}/(\text{kg}\cdot\text{K}), \alpha = 1.56 \cdot 10^{-5} \text{ m}^2/\text{s}\}$ (obtained from EN 1993-1-2:2005 (European Committee for Standardization (2005)) with $k = 54.0 \text{ W}/(\text{m}\cdot\text{K})$) leads to $\mathcal{M}_2 = \{\rho = 3871 \text{ kg}/\text{m}^3, c_p = 770 \text{ J}/(\text{kg}\cdot\text{K}), \alpha = 5.61 \cdot 10^{-6} \text{ m}^2/\text{s}\}$ with $k = 16.7 \text{ W}/(\text{m}\cdot\text{K})$. The material properties for the generative model are summarized in Table 2.

Table 2: Material properties used for the generative model of the thermal application case

| Material Model | Density ρ [kg/m ³] | Heat Capacity c_p [J/(kg·K)] | Conductivity k [W/(m·K)] | Diffusivity α [m ² /s] | Volumetric Fraction f |
|------------------------------|-------------------------------------|--------------------------------|----------------------------|--|-------------------------|
| \mathcal{M}_1^* | 2300 | 900 | 2.0 | 9.66×10^{-7} | 0.717 |
| $\mathcal{M}_{\text{steel}}$ | 7850 | 440 | 54.0 | 1.56×10^{-5} | 0.283 |
| \mathcal{M}_2 | 3871 | 770 | 16.7 | 5.61×10^{-6} | - |

In a real application, it would not be possible to obtain direct measurements of the heat $\dot{Q}_{\text{objective}}$ to infer the value of α in \mathcal{M}_1 . It is more common to have available temperature readings from sensors installed inside or at the surface of the concrete specimen. Four temperature sensors T_i for $i = \{1, 2, 3, 4\}$ are placed into the system as in Figure 16 at the coordinates from Table 3. The sensors in the generative model will provide temperature measurements that at a rate of one sample every 5 min for the first 270 min that will be used to infer the latent parameters. Analogous sensors are defined in the computational model at the same positions. Their observations will be compared during the inference procedure with those collected from the generative model.

Table 3: Sensor coordinates for the thermal application case

| Sensor | X [m] | Y [m] |
|--------|-------|-------|
| T_1 | 0.15 | 0.30 |
| T_2 | 0.30 | 0.30 |
| T_3 | 0.15 | 0.12 |
| T_4 | 0.30 | 0.12 |

Equation 65 is solved over the system to obtain temperature measurements at the sensors. To this end, a finite element (FE) solution is implemented. For simplicity, the geometry is discretized in a regular mesh of 20×20 first-degree Lagrange elements. The thermal problem is solved using a linear solver with the corresponding boundary conditions. The time integration is performed through a forward Euler scheme with 5 min timesteps, which is adequate for the slow evolution of the temperature profile in concrete. The same implementation is used to derive the temperature field to calculate the heat flux through the system. The first 29 min will be used as a transitory regime where the external temperature linearly ramps up starting from 273 K (the same temperature as the system) to 303K. Afterwards, the external temperature is composed by a constant component of 303K and an additional component that simulates variable external conditions. This variable component is composed by a short-term noise sampled at every timestep from a distribution $\mathcal{N}(0K, 1.0K)$ and long-term component that is sampled once every five timesteps from a distribution $\mathcal{N}(0K, 10.0K)$ and interpolated in for the timesteps in between for a smooth transition. Notice that these additional noise components in the temperature are only considered in the data generation, with the isotropic computational model assuming constant external temperature, creating an additional source of model discrepancy. The training and full temperature series are plotted in Figure 17 A comparison of the resolved temperature field at $t = 20$ min is shown in Figure 18.

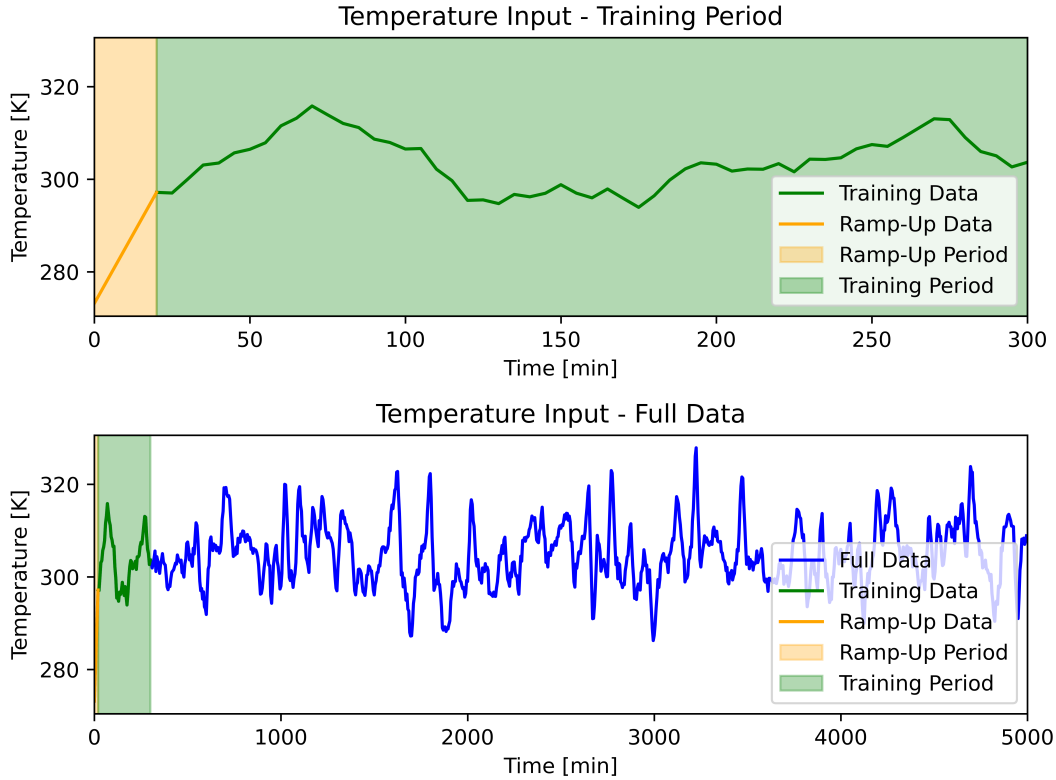


Figure 17: External temperature series for the reinforced concrete thermal example. Training series (top) and full temperature series (bottom) for QoI evaluation.

The solution of the application consists of two parts: the inference of the material parameters from the temperature measurements and the prediction of the heat flux through the midline section over time. Only thanks to the embedding it is possible to quantify the uncertainty in the heat due to the bias that stems from the misspecification of the forward model compared to the generative process.

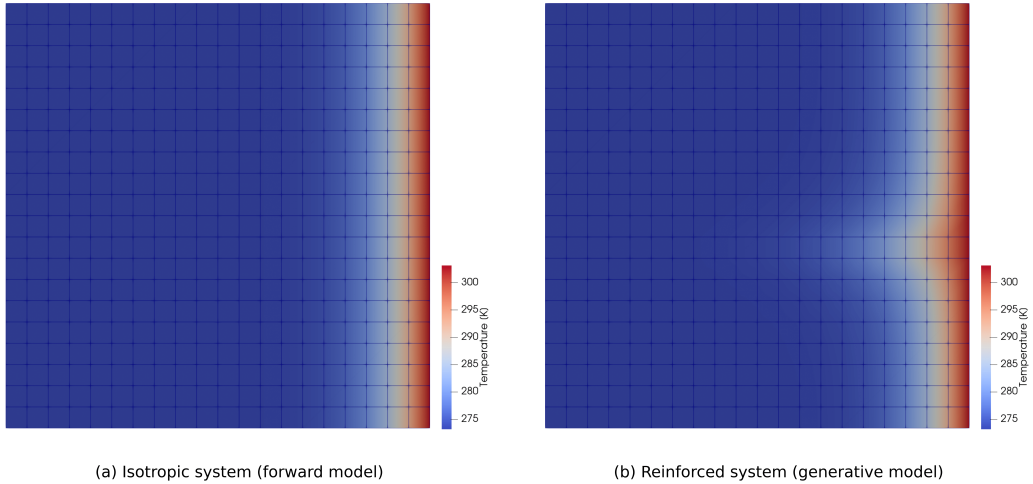


Figure 18: Resolved temperature field at $t = 20$ min. (a) System with isotropic material properties \mathcal{M}_1 and (b) system with a band with modified material properties \mathcal{M}_2 that represent the appearance of a reinforcement bar in that region. The isotropic system presents a uniform temperature gradient from right ($T = 303$ K) to left, while the reinforced system presents a faster development of the temperature front at the position of the reinforcement than in the rest of the system

3.2.1 Temperature inference

To infer the diffusivity α of \mathcal{M}_1 , an MCMC algorithm is implemented. A training dataset will be used for the parameter estimation and an additional testing dataset will be used for validation. The training dataset \mathbf{y} corresponds to the measurements of $T = [T_1 \ T_2 \ T_3 \ T_4]$ between $t=20$ min and $t=220$ min using the generative model with the reinforcement. The first 20 min have been rejected as they belong to the ramp-up phase and the interest is on the stationary regime. A white noise perturbation with $\sigma_N = 0.2$ K is prescribed at the output. For the testing dataset, the simulation is repeated, gathering measurements between $t=20$ min and $t=270$ min.

The embedding for the diffusivity is defined as

$$\alpha = \alpha_m + \delta_b, \quad \delta_b \sim \mathcal{N}(0, \sigma_b^2), \quad (72)$$

where α_m and σ_b are the latent parameters that must be estimated by solving the inverse problem. The prior distributions are $\pi(\alpha_m) \sim \mathcal{N}(10^{-6}, (10^{-7})^2)$ and $\pi(\sigma_b) \sim \mathcal{LN}(-16, 0.1)$. The PCE for computing the forward model with the embedding consist of a Hermite polynomial expansion of degree 2. The noise σ_N is properly specified with a value of 0.2. The MCMC algorithm is run until convergence with a threshold of $\widehat{ESS} = 837$ after 250 steps of burn-in. The results for the ABC likelihood are presented in Figure 19 and for the other likelihoods in D. The summarized inference results are presented in Table 4.

Table 4: Posterior results for the thermal model and different likelihoods

| Likelihood | α_m | | | σ_b | | |
|------------|------------|----------|------|------------|----------|-----|
| | Mean | Std | ESS | Mean | Std | ESS |
| ABC | 1.31e-06 | 2.55e-09 | 847 | 2.37e-07 | 3.43e-09 | 863 |
| GMM | 1.28e-06 | 2.39e-08 | 911 | 1.27e-07 | 1.28e-08 | 864 |
| RGMM | 1.28e-06 | 1.72e-08 | 1009 | 1.70e-07 | 1.06e-08 | 848 |
| IN | 1.27e-06 | 1.51e-08 | 897 | 1.87e-07 | 8.84e-09 | 845 |

The results do not present considerable variations between likelihood models for this case. As the noise is well prescribed, the data points with low sensitivity to changes in the parameters are not used for the training and the model can cover reasonably well the bias in the model, all likelihood models produce roughly equivalent results. The posterior response is able to cover the test data points as well as the training ones thanks to the embedding being included in the latent variable itself. However, the values obtained for α_m with mean between 5×10^{-7} and 6×10^{-7} are not centered at 9.66×10^{-7} , concrete's diffusivity value. This is expected, as there is a bias between the generative system and the computational model, although the real value is included in the range of $\hat{\alpha}_m \pm \hat{\sigma}_b$. The prescribed noise cannot explain the observed temperature measurements, therefore the embedded bias is justified. Inferring the noise scale σ_N with an additive model would have allowed to explain

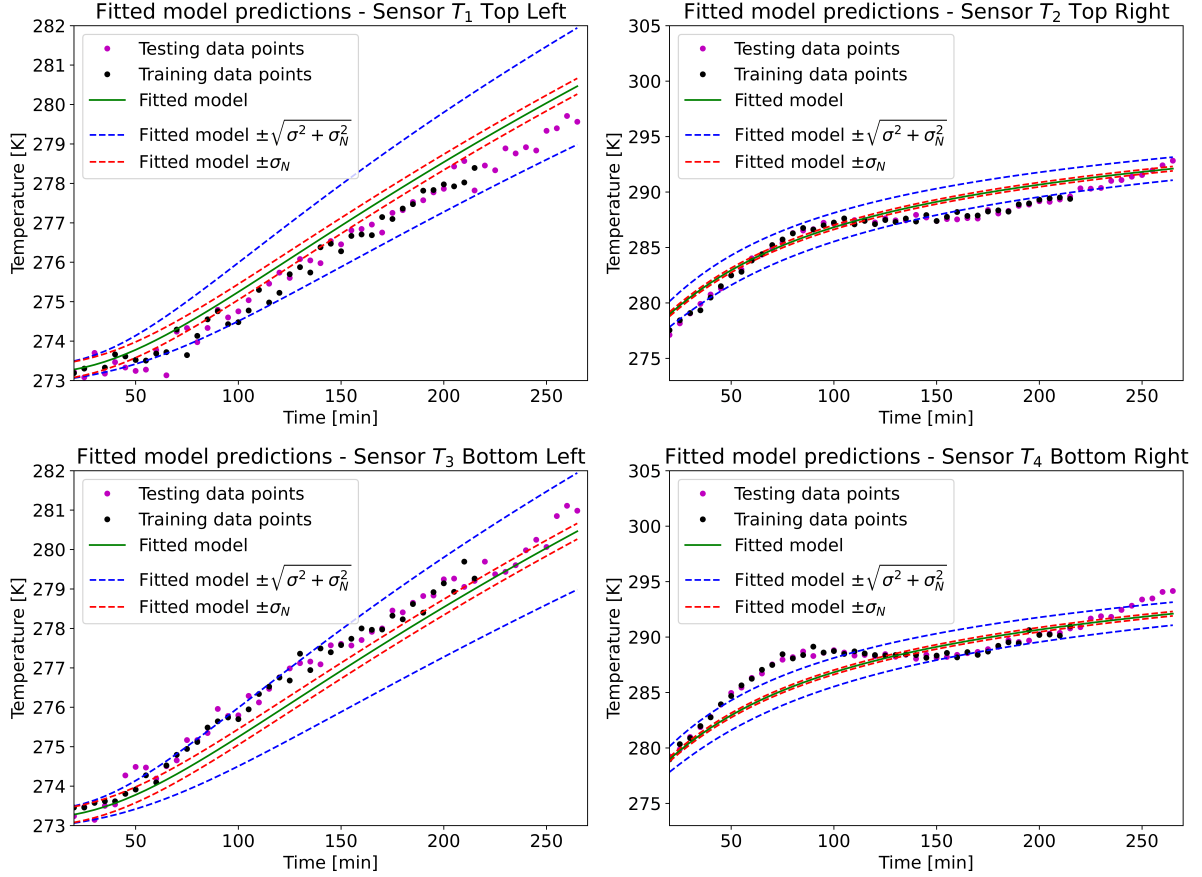


Figure 19: Temperature sensors predictions for ABC likelihood

the variance in the data points as a perturbation in the output, but would not necessarily be able to explain the variance in the testing range. Classical solutions to this case, such as non-additive or heteroscedastic could achieve better results for the prediction of temperature values, but they would not be transferable to heat computations. An analogous situation occurs with the bias formulated following approaches based on Kennedy and O’Hagan’s framework (Kennedy and O’Hagan (2001)), as shown in Andrés Arcones et al. (2024).

3.2.2 Heat prediction

Once the posterior distribution of the latent variables α_m and σ_b are estimated by solving the inverse problem, the updated system is used to calculate the cumulative heat through the cross-section. The simulation is run with the full external temperature series of 5000 min, which allows the development of the full thermal profile. Analogously with the simple example, four QoI are for $t = 5000$ min are evaluated: the output $Q_{\text{obj}}(t = 5000 \text{ min})$, the mean of the predictive distribution μ_P^h , the standard deviation σ_P^h and z-value with a confidence of 95% for $Q_{\text{obj}}(t = 5000 \text{ min})$. The predicted response taking the mean values of the posterior distribution and $\hat{\alpha}_m$ and $\hat{\sigma}_b$ solving Equation with them is presented in Figure 20. The propagated posterior distributions of the QoI are plotted in Figure 21. As observed in Figure 20, the posterior distributions generated by the embeddings are able to reliably envelop the real cumulative heat value. Such is the case due to the similar sources of discrepancy affecting the QoI calculation and the model updating, i.e. heterogeneity in the material and variations in the external temperature. If the heat simulation presented different sources of discrepancy, such as larger temperature variations, the predicted distributions may not be able to reflect the true values. Nevertheless, they always provide a more informative assessment on the reliability of the model predictions. In comparison, the prediction when no bias term is included differs from the true value by more than 10 kJ despite not providing a significant confidence interval, leading to overconfident results.

Analogous conclusions can be extracted from the analysis of the pushed-forward QoIs. While the model without bias produces a point distribution due to the lack of a noise model for the cumulative heat prediction, the embedded models produce distributions that could have generated the true value of 91338 J. This is reflected in the z-values, where all the sampled pairs of latent parameters generate distributions that produce z-values significantly smaller than 1.96. Due to its almost zero variance in the posterior distribution, a z-test would not have been reasonable for the model without bias unless an error model is prescribed. The choice of likelihood

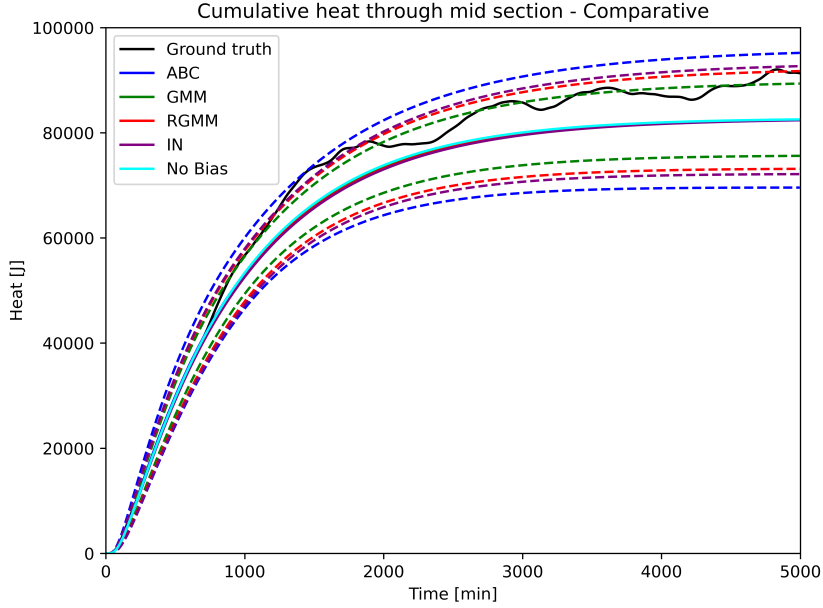


Figure 20: Temperature heat prediction for (a) ABC-likelihood, (b) GMM likelihood, (c) RGMM likelihood, and (d) IN likelihood

does not impact significantly the mean value of the predictions μ_P^h , laying between 82300 and 82550 J. The main difference resides in the value for σ_P^h and the spread of the distributions for each QoI. In general, ABC produces larger distributions of Q_{obj} , with more concentrated values for μ_P^h and σ_P^h . RGMM and IN provide comparable results with each other with a more concentrated Q_{obj} but larger dispersion in the rest of the QoI. Finally, GMM has the largest uncertainty in the pushed-posterior distributions of the QoI despite having providing the Q_{obj} prediction with the smallest variance.

4 Conclusions

This paper has introduced several significant advances in the implementation of embedded bias approaches for quantifying model uncertainties. First, a more interpretable embedding representation was developed as an alternative to the one presented by Sargsyan et al. (2019). Although this approach requires specifying a distribution for the discrepancy, it reduces the dimensionality of the Polynomial Chaos Expansion (PCE) needed to describe the embedding and improves the separation between fitting the embedding's PCE and inferring the model parameters. Next, it was demonstrated that the Approximate Bayesian Computation (ABC) likelihood formulation, commonly used to update model parameters with an embedded bias, is highly sensitive to the prescribed measurement noise and requires careful selection of the parameters γ and ϵ . One of the main contributions of this work is the explicit treatment and analysis of measurement noise, which had previously been mentioned in past studies but not thoroughly examined. To address this, the ABC likelihood was extended to properly account for measurement noise and accurately quantify predictive variance by imposing $\gamma = \sqrt{\pi/2}$. Additionally, two alternative likelihood formulations —Global Moment-Matching (GMM) and Relative Global Moment-Matching (RGMM)— were proposed to mitigate sensitivity issues. These formulations were analyzed and compared against the modified ABC likelihood and the independent normal noise formulation using simple linear and complex transient thermal examples. Finally, a key contribution of this paper is the analysis of how the uncertainties quantified through the embedding approach propagate to Quantities of Interest (QoI) calculated using the updated model and parameters.

The inclusion of the embedded bias term enables the quantification of uncertainty arising during parameter updating due to modeling assumptions, potentially capturing the full range of uncertainties in the measured observations. By introducing the embedding bias term as a stochastic extension of the latent parameters, the proposed formulation allows for straightforward propagation of these uncertainties to other predicted QoIs that depend on the same model parameters. However, as shown in this work, the prescribed measurement noise critically influences the selection of the appropriate likelihood formulation and affects the convergence of the Bayesian updating process when an embedding is used. In particular, ABC likelihoods have been identified as the most sensitive to poor noise prescriptions. Additionally, the embedded bias formulation limits predictions to the range of responses that the model is capable of producing. As a result, discrepancies that cannot be explained by changes in the model parameters, such as offsets or outlier values, can skew the inferred parameters. ABC

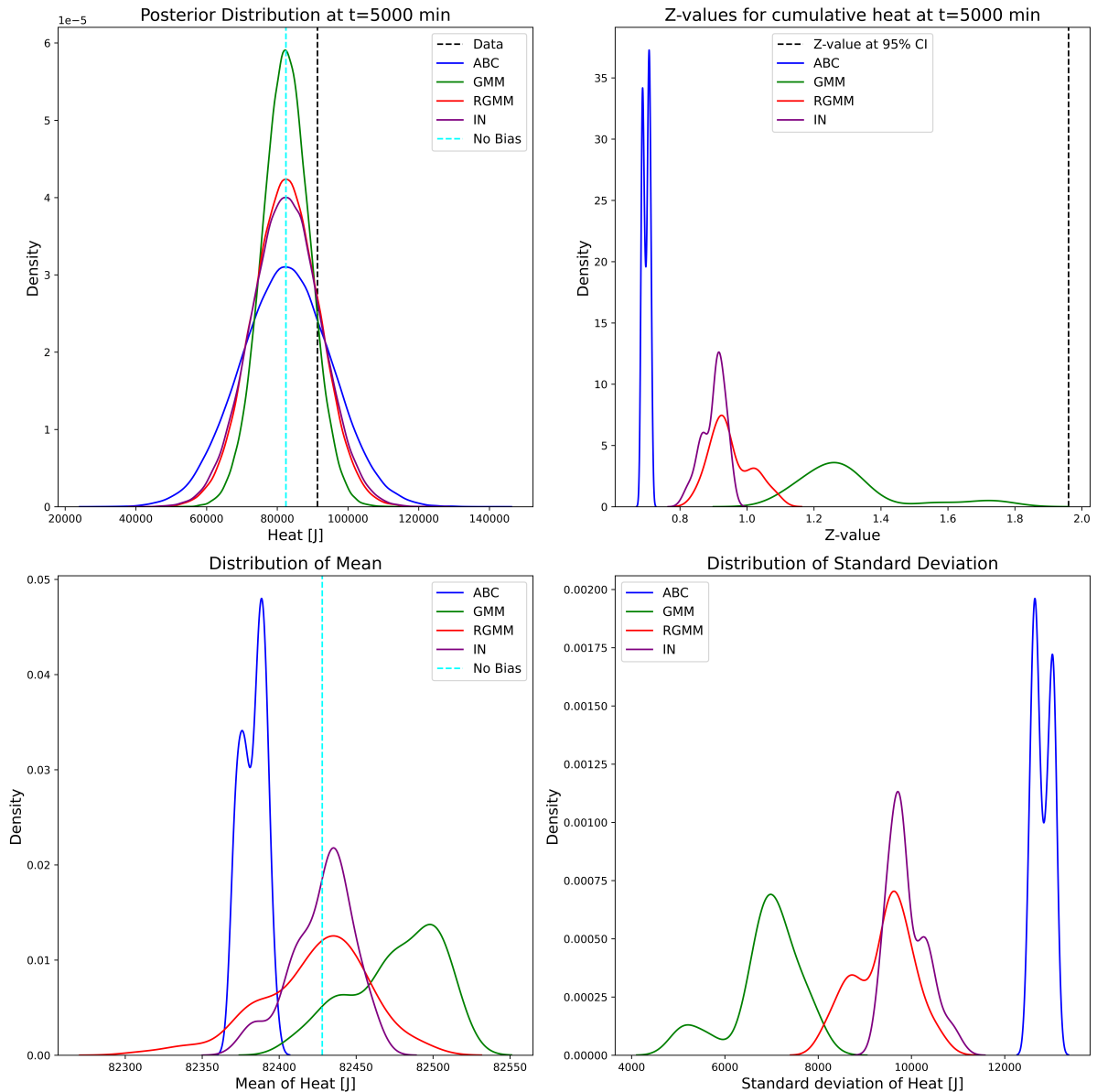


Figure 21: Analysis of Quantities of Interest by propagating the posterior distribution of α and σ_b for the thermal example

methods tend to be more sensitive to outliers, while RGMM and IN are more impacted by offsets or outliers near values with low variance. GMM, on the other hand, is reliable only if the assumption of normality in the residuals is valid. Identifying which of these effects are present during model updating is not always possible and often depends on data analysis or practitioner experience. However, selecting the right likelihood function is crucial in certain cases. Regardless of the chosen likelihood formulation, the inclusion of embedded bias improves predictive posterior distributions, allowing for more informed decision-making, albeit at the cost of increased computational effort during the update phase. While hierarchical Bayesian approaches can produce comparable results when the conditional distributions of the hierarchical formulation are known, a thorough comparison between these methodologies is left for future work.

One of the key strengths of this methodology is its ability to propagate the uncertainty captured by the embedded bias. This paper has demonstrated how propagating the full posterior distribution of the latent parameters through QoI calculations provides insights that are not possible with point estimates or bias-free formulations. Generating distributions for the statistical moments of the predicted QoI enables the use of inference techniques for a more robust analysis of the results. Moreover, the interpretable embedding formulation proposed here allows the propagation of uncertainties related only to specific parameters that influence the QoI being calculated. Nevertheless, when multiple parameters are inferred alongside an associated model bias, it is likely that their biases will be correlated. Implementing and propagating such correlation structures to QoIs where only certain

parameters are relevant remains an open challenge.

In conclusion, the advances presented in this paper represent a significant step toward more effective quantification and propagation of uncertainties in model parameters through embedded bias approaches. One of the main contributions of this work is the explicit consideration and analysis of measurement noise, which had been previously acknowledged in past methods but never thoroughly examined in terms of its impact on the model updating process. Future work should focus on further validating this methodology by applying it to real measurement data from sensors to assess its practical applicability. Additionally, extending the current approach to hierarchical Bayesian formulations and exploring the propagation of correlated biases to various QoIs are important avenues for continued research. These developments promise to enhance the robustness and reliability of uncertainty quantification in complex models.

A Monte Carlo-Markov Chain stopping criteria

In this paper, the MCMC sampler based on ensembles of chains implemented in `emcee` (Foreman-Mackey et al. (2013)) is used for the Bayesian updating framework. In the chosen implementation, a stretch move as defined in Goodman and Weare (2010) proposes the new samples for the next iteration of the MCMC algorithm based on the current values of the ensemble of chains. The chains in a given ensemble are therefore not independent. This correlation invalidates the use of those convergence criteria that are based on the independence of the chains such as Gelman-Rubin's \hat{R} metric (Gelman and Rubin (1992); Vats and Knudson (2021)). Alternatively, the integrated autocorrelation time τ_∞ (Sokal (1997)) quantifies how long it takes for the values in a chain or ensemble to become effectively uncorrelated with one another and is in practice a metric of the quality of the ensemble that does not require independence of the chains. A stopping criteria based on the effective sample size ESS obtained from τ_∞ is imposed on the MCMC algorithm to determine the number of iterations that must be evaluated.

First, an objective ESS threshold must be defined to determine when the chain is converged. Following Vats et al. (2019), an estimated \widehat{ESS} such that

$$\widehat{ESS} \geq W_{p,\alpha,\epsilon} \quad (73)$$

is calculated a priori. The value $W_{p,\alpha,\epsilon}$ depends only on the dimensionality of the problem p , the level of confidence α of the considered regions and the desired precision ϵ . For large samples, i.e. sufficiently long chains, Vats et al. (2019) prove that a good approximation for $W_{p,\alpha,\epsilon}$ is

$$\widehat{ESS} \geq W_{p,\alpha,\epsilon} = \frac{2^{2/p}\pi}{(p\Gamma(p/2))^{2/p}} \frac{\chi_{1-\alpha,p}^2}{\epsilon^2}. \quad (74)$$

Additionally, a maximum number of iterations steps n_{\max} is established. Therefore, the MCMC algorithm will be continued while, for a given iteration i ,

$$ESS_i < \frac{2^{2/p}\pi}{(p\Gamma(p/2))^{2/p}} \frac{\chi_{1-\alpha,p}^2}{\epsilon^2} \text{ and } i < n_{\max}. \quad (75)$$

The effective sample size ESS_i is directly related with τ_∞ at iteration i as

$$ESS_i = \frac{n_i m}{\tau_\infty}, \quad (76)$$

where n_i is the number of steps at iteration i and m is the number of walkers, i.e. chains in the ensemble. In practice, τ_∞ is approximated by an estimation following the implementation described in Sokal (1997). To avoid excessive computations, ESS_i is not calculated after every sample of the MCMC algorithm but after a batch of iterations with predefined size have been evaluated. The MCMC will be stopped when the thresholds of Equation 75 are overpassed for the chains of each latent parameter θ that is being sampled.

B Convergence in moment-matching likelihood with measurement noise

The subsequent demonstration of the convergence of moment-matching likelihoods with a noise model and the extension using sufficient statistics in place of the variables have been adapted from Wilkinson (2013). From Equation 1, the noise model can be expressed as

$$\varepsilon_{\text{noise}} = y - z \quad (77)$$

where $\varepsilon_{\text{noise}}$ follows a zero-mean normal distribution with prescribed variance $\varepsilon_{\text{noise}} \sim \mathcal{N}(0, \sigma_N)$. In case the model response is considered unbiased, i.e. $\varepsilon_{\text{model}} \stackrel{!}{=} 0$, then $\varepsilon_{\text{noise}} = y - f(\theta)$. This assumption corresponds to the belief that the computational model can represent the system response in its totality.

First, we define the random variable Y from which the observations y are realizations. Its probability given a model sample is

$$\pi(Y = y|f(\theta) = z, \theta) = \pi_\varepsilon(y - z) \quad (78)$$

where $\pi_\varepsilon(y - z)$ is the probability associated with a Gaussian likelihood according to the distribution of $\varepsilon_{\text{noise}}$, which follows from Equation 77. Assuming summary statistics $T(\cdot)$ and $t(\cdot)$, *sufficiency* in a Bayesian context (Bernardo and Smith (1994)) is formulated, for almost every x , as

$$\pi(\theta|X = x) = \pi(\theta|T(X) = t(x)), \quad (79)$$

which directly allows to formulate the noise error model from Equation 78 with sufficient statistics as

$$\pi(T(Y) = t(y)|T(f(\theta)) = t(z), \theta) = \pi_\varepsilon(t(y) - t(z)). \quad (80)$$

To simplify notation, the convergence will be proven using the original variables y and $z = f(\theta)$ but can be directly extended with the statistical moments. To define the posterior distribution of θ , Bayes' theorem is applied using the predictions z as auxiliary variable:

$$\pi(\theta, z|y) = \frac{\pi(y|\theta, z)\pi(\theta, z)}{\pi(y)} \quad \text{Bayes' theorem} \quad (81)$$

$$\propto \pi(y|\theta, z)\pi(\theta, z) \quad (82)$$

$$\propto \pi(y|\theta, z)\pi(z|\theta)\pi(\theta) \quad \text{conditioning on } \theta \quad (83)$$

$$\propto \pi(Y = y|f(\theta) = z, \theta)\pi(z|\theta)\pi(\theta) \quad (84)$$

$$\propto \pi_\varepsilon(y - z)\pi(z|\theta)\pi(\theta) \quad \text{from Equation 78} \quad (85)$$

$$\propto \pi_\varepsilon(y - z)\pi(\theta) \quad \text{if } f(\theta) \text{ is deterministic.} \quad (86)$$

In this paper, $\pi_\varepsilon(\cdot)$ is from an exponential family, denoting Gaussian noise. When summary statistics are involved, composed error models are possible. For example, a valid formulation would be

$$\pi_\varepsilon(t(y) - t(z)) = \pi_{t_1}(t_1(y) - t_1(z))\pi_{t_2}(t_2(y) - t_2(z)) \quad (87)$$

where π_{t_1} and π_{t_2} are the respective noise models for the statistics t_1 and t_2 .

Markov chains converge to the aforementioned posterior distribution when using the noisy likelihood (Wilkinson (2013)). In effect, given a transition kernel $q(\theta, \theta')$ defined in the chosen MCMC approach, it must be proven that the *detailed balance equations* are satisfied. Considering $\pi(\cdot)$ the target stationary distribution and $p(\cdot, \cdot)$ the transition kernel of the chain, which also depends on $q(\theta, \theta')$, the detailed balance equations are formulated as

$$\pi(u)p(u, v) = \pi(v)p(v, u) \quad \forall u, v. \quad (88)$$

The transition kernel of the chain is the product between the kernel defined by the MCMC approach and the acceptance rate imposed by the ABC approach. The acceptance ratio for a given proposal represents the probability of accepting a given sample and is defined as

$$r((\theta_t, z_t), (\theta', z')) = \min\left(1, \frac{\pi_\varepsilon(y - z')q(\theta', \theta_t)\pi(\theta')}{\pi_\varepsilon(y - z_t)q(\theta_t, \theta')\pi(\theta_t)}\right) \quad (89)$$

Therefore, the transition kernel is

$$p((\theta_t, z_t), (\theta', z')) = q(\theta_t, \theta')\pi(z'|\theta') \min\left(1, \frac{\pi_\varepsilon(y - z')q(\theta', \theta_t)\pi(\theta')}{\pi_\varepsilon(y - z_t)q(\theta_t, \theta')\pi(\theta_t)}\right) \quad (90)$$

where (θ_t, z_t) define the current state of the chain and (θ', z') , the new sample. The stationary distribution follows from Bayes' theorem and Equations 81-85 as

$$\pi(\theta, z) = \pi(y)\pi(\theta, z|y) = \pi_\varepsilon(y - z)\pi(z|\theta)\pi(\theta). \quad (91)$$

Combining the transition kernel and the stationary distribution, the detailed balance equations are satisfied directly. The current state of the chain $u = (\theta_t, z_t)$ is expressed as

$$\pi(u) = \pi(\theta_t, z_t) = \pi(y)\pi_\varepsilon(y - z_t)\pi(z_t|\theta_t)\pi(\theta_t), \quad (92)$$

and the new sample $v = (\theta', z')$ as

$$\pi(v) = \pi(\theta', z') = \pi(y)\pi_\varepsilon(y - z')\pi(z'|\theta')\pi(\theta'). \quad (93)$$

From the transition kernel defined in Equation 90, $p(u, v)$ is directly the transition probability $p((\theta_t, z_t), (\theta', z'))$, and $p(v, u)$ is its conjugated

$$p(v, u) = p((\theta', z'), (\theta_t, z_t)) = q(\theta', \theta_t)\pi(z_t|\theta_t) \min\left(1, \frac{\pi_\varepsilon(y - z_t)q(\theta_t, \theta')\pi(\theta_t)}{\pi_\varepsilon(y - z')q(\theta', \theta_t)\pi(\theta')}\right). \quad (94)$$

Notice that when $p(u, v) = q(\theta_t, \theta')\pi(z'|\theta')$, then $p(v, u) = q(\theta', \theta_t)\pi(z_t|\theta_t)\frac{\pi_\varepsilon(y-z_t)q(\theta_t, \theta')\pi(\theta_t)}{q(\theta', \theta_t)\pi_\varepsilon(y-z')\pi(\theta')}$ and vice-versa, as the non-constant part of the minimization function of one transition kernel is the inverse of the other. The balance equation from Equation 88 must be evaluated in the two possible cases of the minimization function:

$$\begin{aligned}\pi(u)p(u, v) &= \pi(y)\pi_\varepsilon(y - z_t)\pi(z_t|\theta_t)\pi(\theta_t)q(\theta_t, \theta')\pi(z'|\theta') = \\ &= \pi(y)\pi(z'|\theta')\pi(z_t|\theta_t)\pi_\varepsilon(y - z_t)q(\theta_t, \theta')\pi(\theta_t) = \pi(v)p(v, u),\end{aligned}\tag{95}$$

and

$$\begin{aligned}\pi(u)p(u, v) &= \pi(y)\pi(z_t|\theta_t)\pi(z'|\theta')\pi_\varepsilon(y - z')q(\theta', \theta_t)\pi(\theta') = \\ &= \pi(y)\pi_\varepsilon(y - z')\pi(z'|\theta')\pi(\theta')q(\theta', \theta_t)\pi(z_t|\theta_t) = \pi(v)p(v, u),\end{aligned}\tag{96}$$

which implies the fulfilment of the balance equations and the convergence of the MCMC chain for transition kernels $q(\theta, \theta')$ that are well defined. This derivation holds for the MCMC framework used in this paper, which is based on ensemble samplers with a stretch move.

C Moment-matching likelihood behaviour with measurement noise

Let A_i be the residual at a given point i as $A_i = |\mu_i^h - y_i|$ and B_i the total standard deviation of the model as $B_i = \sqrt{\sigma_N^2 + \sigma_i^{h^2}}$. A_i and B_i are independent of each other, as A_i depends on the value of the original latent parameters and B_i on the value of the auxiliary ones introduced in the embedded bias. Then, the noisy moment-matching likelihood from Equation 26 in its logarithmic form reads

$$\log \mathcal{L}(\theta) = -\frac{n_y}{2} \log(2\pi\epsilon^2\sigma_N^2) - \sum_{i=1}^{n_y} \exp\left(\frac{A_i^2}{2\sigma_N^2} + \frac{(B_i - \gamma A_i)^2}{2\epsilon^2}\right).\tag{97}$$

The goal is to analyze the behaviour of the likelihood function for the different values of A and B , especially for the cases that lead to the optimal values. Obtaining the cases for which increasing or decreasing A or B leads to higher likelihood allows discerning tendencies in the optimization procedure and potential optimums. To do so, the derivatives of the likelihood with respect to A and B are required. Deriving the likelihood with respect to the residuals A_i , we obtain

$$\frac{\partial \log \mathcal{L}}{\partial A} = -\sum_{i=1}^{n_y} \left(\frac{A_i}{\sigma_N^2} - \frac{\gamma(B_i - \gamma A_i)}{\epsilon^2}\right)\tag{98}$$

$$= -\sum_{i=1}^{n_y} \left(\left(\frac{1}{\sigma_N^2} + \frac{\gamma^2}{\epsilon^2}\right)A_i - \frac{\gamma}{\epsilon^2}B_i\right).\tag{99}$$

Positive values of these derivatives imply that an increase of the residuum would produce a larger likelihood, and consequently, a ‘‘worse’’ fit of the mean values is favoured. Analogously, negative values of the derivative with respect to A favour a better fit of the mean values of the prediction with the observations. Alternatively, deriving with respect to the total deviation B_i we obtain

$$\frac{\partial \log \mathcal{L}}{\partial B} = -\sum_{i=1}^{n_y} \frac{\gamma(B_i - \gamma A_i)}{\epsilon^2}\tag{100}$$

$$= -\sum_{i=1}^{n_y} \left(-\frac{\gamma}{\epsilon^2}A_i + \frac{1}{\epsilon^2}B_i\right).\tag{101}$$

In this case, positive values of the derivative with respect to B favour increasing the predicted bias, while negative values favour reducing it. For an analysis of the optimality, the second derivatives have to be computed. The entries of the Hessian matrix $\mathbf{H}(A, B)$ are calculated as

$$\frac{\partial^2 \log \mathcal{L}}{\partial A^2} = -n_y \left(\frac{1}{\sigma_N^2} + \frac{\gamma^2}{\epsilon^2}\right)\tag{102}$$

$$\frac{\partial^2 \log \mathcal{L}}{\partial B^2} = -\frac{n_y}{\epsilon^2}\tag{103}$$

$$\frac{\partial^2 \log \mathcal{L}}{\partial A \partial B} = \frac{\partial^2 \log \mathcal{L}}{\partial B \partial A} = -\frac{\gamma n_y}{\epsilon^2}\tag{104}$$

and its determinant returns

$$\det(\mathbf{H}(A, B)) = \frac{\partial^2 \log \mathcal{L}}{\partial A^2} \frac{\partial^2 \log \mathcal{L}}{\partial B^2} - \frac{\partial^2 \log \mathcal{L}}{\partial A \partial B} \frac{\partial^2 \log \mathcal{L}}{\partial B \partial A} = \frac{n_y^2}{\epsilon^2} \left(\frac{1}{\sigma_N^2} + \frac{\gamma^2}{\epsilon^2}\right) - \frac{\gamma^2 n_y^2}{\epsilon^4} = \frac{n_y^2}{\epsilon^2 \sigma_N^2} > 0.\tag{105}$$

As $\frac{\partial^2 \log \mathcal{L}}{\partial A^2} < 0$ for any allowed value of the parameters, all critical points of $\log \mathcal{L}$ are local maximum. Therefore, the log-likelihood defined is concave as expected and $\frac{\partial \log \mathcal{L}}{\partial A}, \frac{\partial \log \mathcal{L}}{\partial B} > 0$ lead closer to the optimum. Taking means over n_y , it can be observed that

$$\frac{\partial \log \mathcal{L}}{\partial A} > 0 \iff \frac{1}{n_y} \frac{\partial \log \mathcal{L}}{\partial A} > 0 \quad (106)$$

therefore

$$\frac{\partial \log \mathcal{L}}{\partial A} > 0 \iff -\left(\frac{1}{\sigma_N^2} + \frac{\gamma^2}{\epsilon^2}\right) \bar{A} + \frac{\gamma}{\epsilon^2} \bar{B} > 0 \quad (107)$$

where \bar{A} and \bar{B} denote, respectively, the mean value of A and B over the observations. Using the mean value instead of the sum simplifies the analysis and allows for a more direct comparison between cases than using the sum of individual terms. Analogously,

$$\frac{\partial \log \mathcal{L}}{\partial B} > 0 \iff \frac{\gamma}{\epsilon^2} \bar{A} - \frac{1}{\epsilon^2} \bar{B} > 0. \quad (108)$$

Based on this information, the cases indicated in Table 5 are considered. Note that for the likelihood presented in Equation 21, the results will be equivalent by simply taking $\sigma_N^2 = \epsilon^2$. These cases allow for the following interpretations:

1. Case (I) corresponds to the situation where the variance predicted by the model cannot cover the residuals. The resulting tendency assuming an optimal path would be an increase in the predicted variance and a reduction of the residual. This case occurs when the predictions for a given sampled parameter vector are inaccurate or if the variance in the observations is under-represented.
2. Case (II) corresponds to a model that predicts perfectly the variance (on average) as prescribed by the approximated model, while the residuals are not well represented.
3. Case (III) is produced by a model that predicts a larger variance than the one needed to obtain the observations and where the residuum can be reduced. In cases with prescribed noise, further reducing the variance may not be possible.
4. Case (IV) represents the case where the fitting of the residuals is considered optimum. However $\bar{B} = \gamma \bar{A}$ as prescribed only if $\epsilon = 0$. Otherwise, the predicted variation will have to be reduced to achieve the optimum.
5. Case (V) is symmetrical to Case (I), where the model over-represents the variance in the observations. Therefore, the residuals are increased to present a larger variance while the predicted deviation is to be reduced.
6. Case (VI) is a special case of (V) where the model can exactly represent on average the observations. However, $B > 0$ by construction, unless the case without noise or predicted variance is allowed. The residuals will tend to be increased at least up to the minimum possible of the predicted variance.
7. Case (VII) is the actual maximum, which can be achieved only if the predictions and their variance can be predicted exactly by the model. It is a special case of (II) for $\bar{A} = 0$.

Cases (VI) and (VII) are generally not possible in the presence of model discrepancy and noise. The minimum \bar{A} possible is limited by the model discrepancy and the minimum \bar{B} possible is limited by the noise term. Superior limits can only be prescribed manually. If $\min \bar{A} > \min \bar{B}$, then the residual can be covered by the predicted bias, and the optimum will be at Case (II) for $\bar{B} = \gamma \min \bar{A}$. However, if $\min \bar{A} < \min \bar{B}$, the optimum will be at Case (IV) with $\bar{A} = \left(\gamma + \frac{\epsilon^2}{\sigma_N^2}\right)^{-1} \min \bar{B}$. In such a case, the residuals are minimized in order to fit better the predicted variance, which is generally undesirable for a good fit. This situation can be avoided with a proper quantification of the noise and the embedding of the right parameters such that B covers the residuals of A in the most probable range.

Table 5: Cases for noisy moment-matching log-likelihood behaviour

| | Cases | $\frac{\partial \log \mathcal{L}}{\partial A}$ | $\frac{\partial \log \mathcal{L}}{\partial B}$ |
|-------|--|--|--|
| (I) | $\bar{B} < \gamma \bar{A}$ | Negative | Positive |
| (II) | $\bar{B} = \gamma \bar{A}$ | Negative | Zero |
| (III) | $\bar{B} \in \left(\gamma \bar{A}, \left(\gamma + \frac{\epsilon^2}{\sigma_N^2}\right) \bar{A}\right)$ | Negative | Negative |
| (IV) | $\bar{B} = \left(\gamma + \frac{\epsilon^2}{\sigma_N^2}\right) \bar{A}$ | Zero | Negative |
| (V) | $\bar{B} > \left(\gamma + \frac{\epsilon^2}{\sigma_N^2}\right) \bar{A}$ | Positive | Negative |
| (VI) | $\bar{A} = 0, \bar{B} > 0^1$ | Positive | Negative |
| (VII) | $\bar{A} = 0, \bar{B} = 0^2$ | Zero | Zero |

D Results thermal example

The results for Section 3.2.1 for GMM, RGMM and IN likelihoods are presented here.

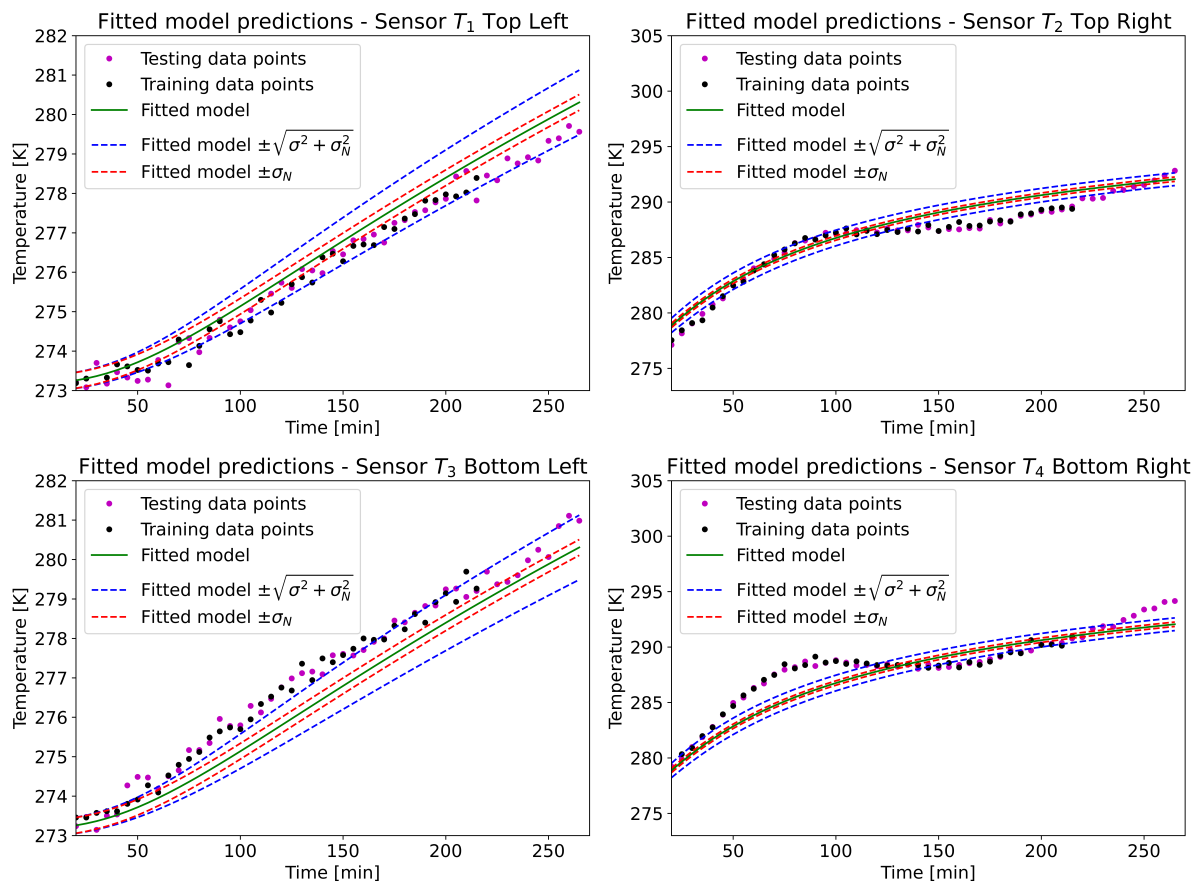


Figure 22: Temperature sensors predictions for GMM likelihood

References

- Andrés Arcones, D., Weiser, M., Koutsourelakis, P.-S., and Unger, J. F. (2023). A bayesian framework for simulation-based digital twins of bridges. *ce/papers*, 6(5):734–740.
- Andrés Arcones, D., Weiser, M., Koutsourelakis, P., and Unger, J. F. (2024). Model bias identification for bayesian calibration of stochastic digital twins of bridges. *Applied Stochastic Models in Business and Industry*.
- Barbillon, P., Forte, A., and Paulo, R. (2024). Screening the discrepancy function of a computer model. *Technometrics*, pages 1–21.
- Bayarri, M. J., Berger, J. O., and Liu, F. (2009). Modularization in bayesian analysis, with emphasis on analysis of computer models. *Bayesian Analysis*, 4(1).
- Bernardo, J. M. and Smith, A. F. M. (1994). *Bayesian theory*. Wiley.
- Bojke, L., Claxton, K., Sculpher, M., and Palmer, S. (2009). Characterizing structural uncertainty in decision analytic models: A review and application of methods. *Value in Health*, 12(5):739–749.
- Brynjarsdóttir, J. and O’Hagan, A. (2014). Learning about physical parameters: the importance of model discrepancy. *Inverse Problems*, 30(11):114007.
- Campbell, K. (2006). Statistical calibration of computer simulations. *Reliability Engineering and System Safety*, 91(10-11):1358–1363.
- Cochran, W. G. (1934). The distribution of quadratic forms in a normal system, with applications to the analysis of covariance. *Mathematical Proceedings of the Cambridge Philosophical Society*, 30(2):178–191.

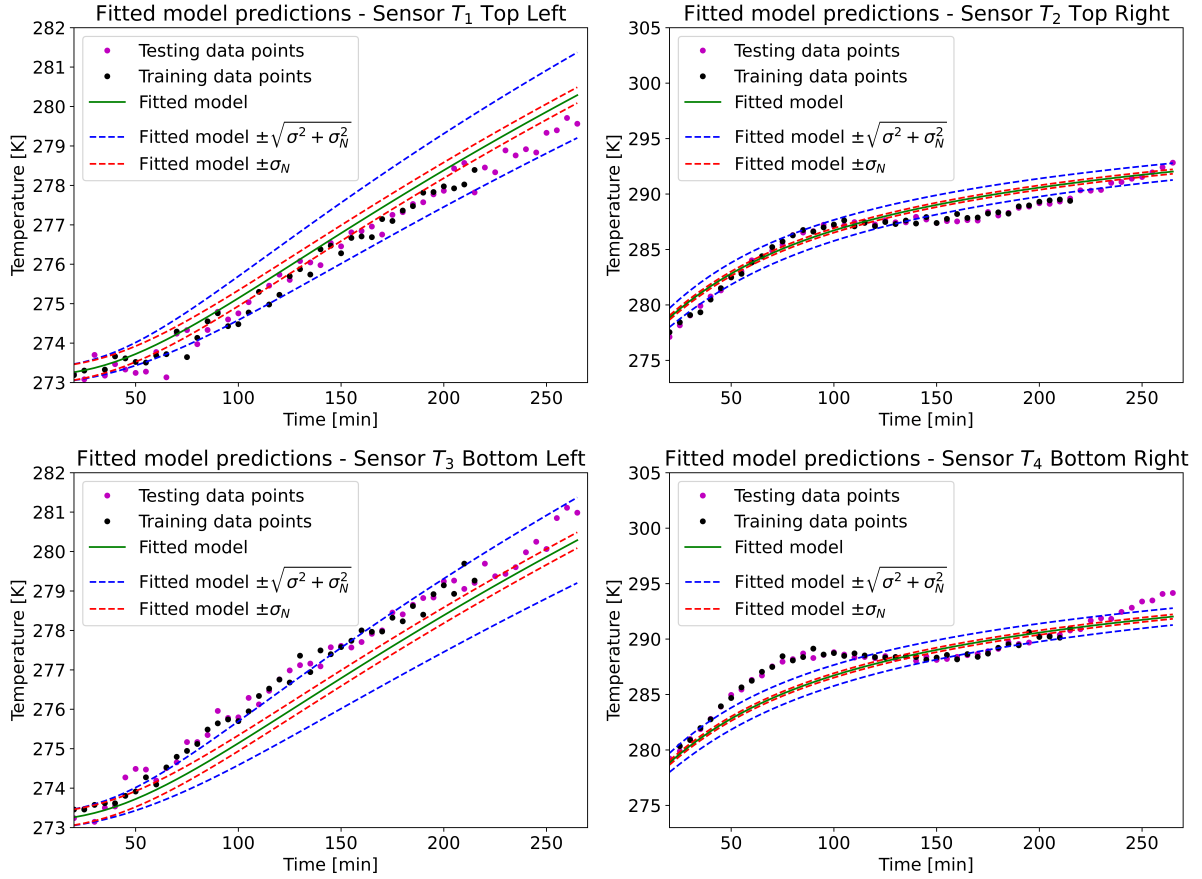


Figure 23: Temperature sensors predictions for RGMM likelihood

- Constantine, P. G., Eldred, M. S., and Phipps, E. T. (2012). Sparse pseudospectral approximation method. *Computer Methods in Applied Mechanics and Engineering*, 229–232:1–12.
- Daly, A. C., Cooper, J., Gavaghan, D. J., and Holmes, C. (2017). Comparing two sequential Monte Carlo samplers for exact and approximate bayesian inference on biological models. *Journal of The Royal Society Interface*, 14(134):20170340.
- Dietz, L. (2010). Directed factor graph notation for generativemodels. Technical report, Max Planck Institute for Informatics.
- European Committee for Standardization (2004). EN 1992-1-1 Eurocode 2: Design of concrete structures - Part 1-2: Structural fire design.
- European Committee for Standardization (2005). EN 1993-1-1 Eurocode 3: Design of steel structures - Part 1-2: General rules - Structural fire design.
- Fearnhead, P. and Prangle, D. (2012). Constructing summary statistics for approximate bayesian computation: Semi-automatic approximate bayesian computation. *Journal of the Royal Statistical Society Series B: Statistical Methodology*, 74(3):419–474.
- Feinberg, J. and Langtangen, H. P. (2015). Chaospy: An open source tool for designing methods of uncertainty quantification. *Journal of Computational Science*, 11:46–57.
- Foreman-Mackey, D., Hogg, D. W., Lang, D., and Goodman, J. (2013). emcee: The MCMC hammer. *Publications of the Astronomical Society of the Pacific*, 125(925):306–312.
- Gelman, A., Carlin, J., Stern, H., Dunson, D., Vehtari, A., and Rubin, D. (2013). *Bayesian Data Analysis*. Chapman and Hall, London, 3 edition.
- Gelman, A. and Rubin, D. B. (1992). Inference from iterative simulation using multiple sequences. *Statistical Science*, 7(4).
- Goodman, J. and Weare, J. (2010). Ensemble samplers with affine invariance. *Communications in Applied Mathematics and Computational Science*, 5(1):65–80.
- Gupta, H. V., Clark, M. P., Vrugt, J. A., Abramowitz, G., and Ye, M. (2012). Towards a comprehensive assessment of model structural adequacy. *Water Resources Research*, 48(8).

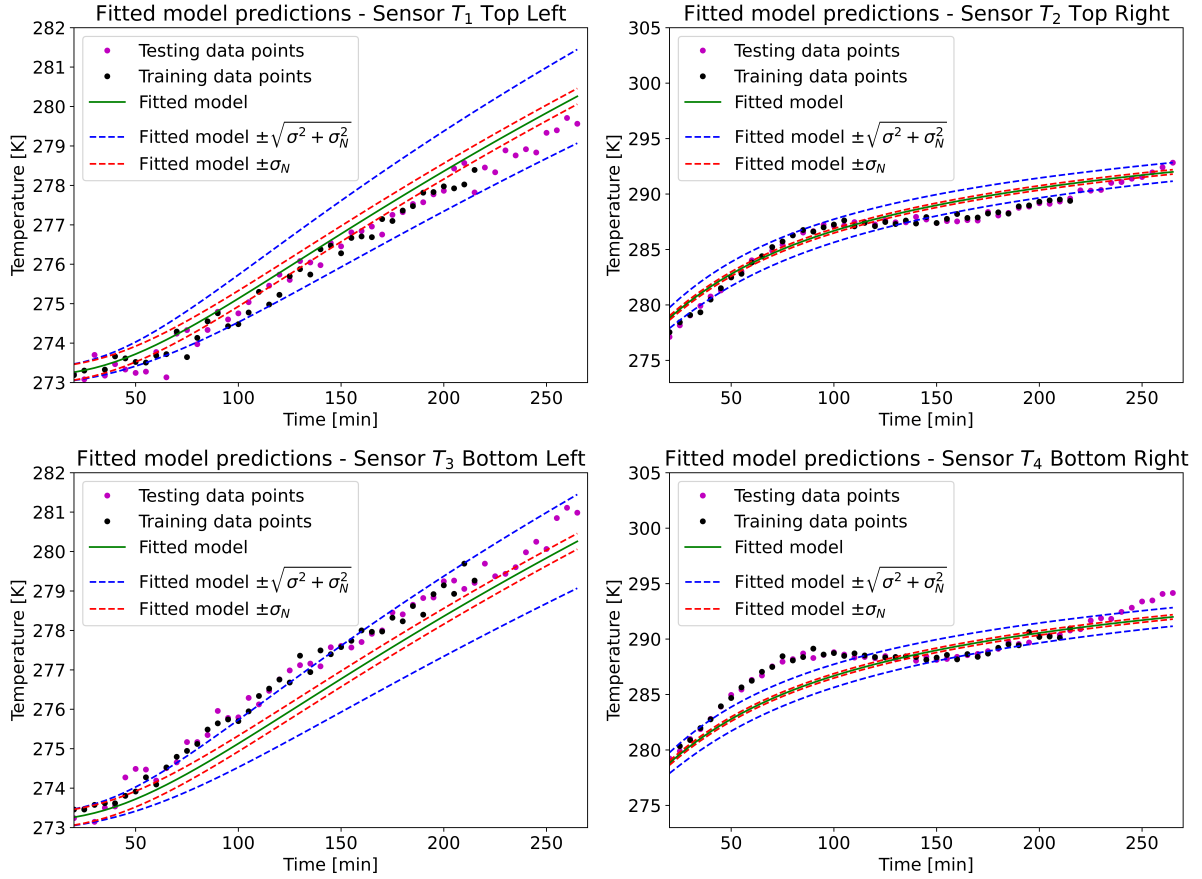


Figure 24: Temperature sensors predictions for IN likelihood

- Huan, X., Safta, C., Sargsyan, K., Geraci, G., Eldred, M. S., Vane, Z., Lacaze, G., Oefelein, J. C., and Najm, H. N. (2017). Global sensitivity analysis and quantification of model error for large eddy simulation in scramjet design. In *19th AIAA Non-Deterministic Approaches Conference*. American Institute of Aeronautics and Astronautics.
- Jakeman, J. D., Franzelin, F., Narayan, A., Eldred, M., and Plfüger, D. (2019). Polynomial chaos expansions for dependent random variables. *Computer Methods in Applied Mechanics and Engineering*, 351:643–666.
- John, D. N. (2021). *Uncertainty quantification for an electric motor inverse problem - tackling the model discrepancy challenge*. PhD thesis, Heidelberg University.
- John, D. N., Stohrer, L., Schillings, C., Schick, M., and Heuveline, V. (2021). Hierarchical surrogate-based approximate bayesian computation for an electric motor test bench.
- Kaipio, J. and Somersalo, E. (2006). *Statistical and Computational Inverse Problems*. Springer London, Limited.
- Kennedy, M. C. and O’Hagan, A. (2001). Bayesian calibration of computer models. *Journal of the Royal Statistical Society: Series B (Statistical Methodology)*, 63(3):425–464.
- Kleijn, B. and van der Vaart, A. (2012). The Bernstein-Von-Mises theorem under misspecification. *Electronic Journal of Statistics*, 6(none).
- Leone, F. C., Nelson, L. S., and Nottingham, R. B. (1961). The folded normal distribution. *Technometrics*, 3(4):543–550.
- Leoni, N., Maître, O. L., Rodio, M.-G., and Congedo, P. M. (2024). Bayesian calibration with adaptive model discrepancy. *International Journal for Uncertainty Quantification*, 14(1):19–41.
- Li, Q., Du, X., Ni, P., Han, Q., Xu, K., and Bai, Y. (2024). Improved hierarchical bayesian modeling framework with arbitrary polynomial chaos for probabilistic model updating. *Mechanical Systems and Signal Processing*, 215:111409.
- Marjoram, P., Molitor, J., Plagnol, V., and Tavaré, S. (2003). Markov chain Monte Carlo without likelihoods. *Proceedings of the National Academy of Sciences*, 100(26):15324–15328.

- Mortensen, J. J., Kaasbjerg, K., Frederiksen, S. L., Nørskov, J. K., Sethna, J. P., and Jacobsen, K. W. (2005). Bayesian error estimation in density-functional theory. *Phys. Rev. Lett.*, 95:216401.
- Obermeyer, F., Bingham, E., Jankowiak, M., Pradhan, N., Chiu, J., Rush, A., and Goodman, N. (2019). Tensor variable elimination for plated factor graphs. In Chaudhuri, K. and Salakhutdinov, R., editors, *Proceedings of the 36th International Conference on Machine Learning*, volume 97 of *Proceedings of Machine Learning Research*, pages 4871–4880. PMLR.
- Oliver, T. A., Terejanu, G., Simmons, C. S., and Moser, R. D. (2015). Validating predictions of unobserved quantities. *Computer Methods in Applied Mechanics and Engineering*, 283:1310–1335.
- Pernot, P. (2017). The parameter uncertainty inflation fallacy. *The Journal of Chemical Physics*, 147(10).
- Pernot, P. and Cailliez, F. (2017). A critical review of statistical calibration/prediction models handling data inconsistency and model inadequacy. *AIChE Journal*, 63(10):4642–4665.
- Plumlee, M. (2017). Bayesian calibration of inexact computer models. *Journal of the American Statistical Association*, 112(519):1274–1285.
- Prangle, D. (2017). Adapting the ABC distance function. *Bayesian Analysis*, 12(1).
- Robert, C. P. (2007). *The Bayesian Choice*. Springer.
- Robert, C. P. and Casella, G. (2004). *Monte Carlo Statistical Methods*. Springer New York.
- Sargsyan, K., Huan, X., and Najm, H. N. (2019). Embedded model error representation for bayesian model calibration. *International Journal for Uncertainty Quantification*, 9(4):365–394.
- Sargsyan, K., Najm, H. N., and Ghanem, R. (2015). On the statistical calibration of physical models. *International Journal of Chemical Kinetics*, 47(4):246–276.
- Schälte, Y. and Hasenauer, J. (2020). Efficient exact inference for dynamical systems with noisy measurements using sequential approximate bayesian computation. *Bioinformatics*, 36(Supplement 1):i551–i559.
- Shen, Z., Brooks, A. L., He, Y., Shrestha, S. S., and Zhou, H. (2021). Evaluating dynamic thermal performance of building envelope components using small-scale calibrated hot box tests. *Energy and Buildings*, 251:111342.
- Sisson, S., Fan, Y., and Beaumont, M., editors (2018). *Handbook of Approximate Bayesian Computation*. Chapman and Hall/CRC, first edition.
- Sisson, S. A. and Fan, Y. (2010). Likelihood-free MCMC. In Brooks, S., Gelman, A., Jones, G., and Meng, X.-L., editors, *Handbook of Markov Chain Monte Carlo*. Chapman and Hall/CRC.
- Sokal, A. (1997). Monte Carlo methods in statistical mechanics: Foundations and new algorithms. In DeWitt-Morette, C., Cartier, P., and Folacci, A., editors, *Functional Integration*, pages 131–192. Springer US.
- Strong, M. and Oakley, J. E. (2014). When is a model good enough? Deriving the expected value of model improvement via specifying internal model discrepancies. *SIAM/ASA Journal on Uncertainty Quantification*, 2(1):106–125.
- Sudret, B. (2021). Polynomial chaos expansions in 90 minutes.
- Sung, C. and Tuo, R. (2024). A review on computer model calibration. *WIREs Computational Statistics*, 16(1).
- Turner, B. M. and Van Zandt, T. (2013). Hierarchical approximate bayesian computation. *Psychometrika*, 79(2):185–209.
- Vaidya, S., Ambad, P., and Bhosle, S. (2018). Industry 4.0 – a glimpse. *Procedia Manufacturing*, 20:233–238.
- van der Vaart, A. W. (2000). *Asymptotic Statistics*. Cambridge University Press.
- Vats, D., Flegal, J. M., and Jones, G. L. (2019). Multivariate output analysis for Markov chain Monte Carlo. *Biometrika*, 106(2):321–337.
- Vats, D. and Knudson, C. (2021). Revisiting the Gelman-Rubin diagnostic. *Statistical Science*, 36(4).
- Walker, W., Harremoës, P., Rotmans, J., van der Sluijs, J., van Asselt, M., Janssen, P., and Kraayer von Krauss, M. (2003). Defining uncertainty: A conceptual basis for uncertainty management in model-based decision support. *Integrated Assessment*, 4(1):5–17.
- Wang, Z., Qiao, Y., Liu, Y., Bao, J., Gao, Q., Chen, J., Yao, H., and Yang, L. (2021). Thermal storage performance of building envelopes for nearly-zero energy buildings during cooling season in western china: An experimental study. *Building and Environment*, 194:107709.
- Wilkinson, R. D. (2013). Approximate bayesian computation (ABC) gives exact results under the assumption of model error. *Statistical Applications in Genetics and Molecular Biology*, 12(2).
- Wu, J.-L., Levine, M. E., Schneider, T., and Stuart, A. (2024). Learning about structural errors in models of complex dynamical systems. *Journal of Computational Physics*, page 113157.
- Xiu, D. and Karniadakis, G. E. (2002). The Wiener–Askey polynomial chaos for stochastic differential

equations. *SIAM Journal on Scientific Computing*, 24(2):619–644.